# Exploring Dynamics in the Far-Infrared with Terahertz Spectroscopy

Charles A. Schmuttenmaer

*Department of Chemistry, Yale University, 225 Prospect Street, P.O. Box 208107, New Haven, Connecticut 06520-8107*

*Received September 4, 2003*

## *Contents*



Charles Schmuttenmaer is Professor of Chemistry at Yale University. He was born and raised in Oak Park, IL. He received a B.S. in chemistry from the University of Illinois in 1985, and a Ph.D. from the University of California, Berkeley, in 1991 under the guidance of Richard J. Saykally. He spent 3 years as a postdoctoral fellow at the University of Rochester under the direction of James M. Farrar and R. J. Dwayne Miller before joining the Yale faculty in 1994. His research has focused on novel applications of time-resolved terahertz (far-infrared) spectroscopy, or TRTS. In particular, he has exploited the unique features of this recent experimental development to explore dynamics in liquids, and transient photoconductivity in semiconductors, quantum dots, and nanoparticles always gaining information that cannot be obtained in any other manner. He is a member of the American Chemical Society, American Physical Society, Optical Society of America, and American Association for the Advancement of Science.

## *1. Introduction and Background*

Chemical and physical systems undergoing change display spectral signatures from the radio frequency to the X-ray region of the electromagnetic spectrum. This has led to the development of time-resolved spectroscopic tools across this entire range, with some emerging more recently than others. This review will focus on time-resolved terahertz (THz) spectroscopy. Throughout this review, the terms "terahertz" and "far-infrared" (FIR) can be used interchangeably. THz spectroscopy covers the region from 0.3 to 20 THz (from 10 to 600 $cm^{-1}$), with most of the work being done between 0.5 and 3 THz. When converted to other units, 1 THz is equivalent to 33.33 $cm^{-1}$ (wavenumbers), 0.004 eV photon energy, or 300 $\mu$m wavelength.

The fact that THz pulses are created and detected using short-pulsed lasers with pulse widths ranging from ∼100 down to ∼10 fs adds a new element that is not present in conventional far-IR studies: It is now possible to carry out *time-resolved* far-IR studies with subpicosecond temporal resolution. In contrast, other sources of far-IR radiation such as arc lamps or globars are continuous, and pulsed sources such as free electron lasers or synchrotrons typically produce far-IR pulses with ∼3 ps duration or greater. An additional advantage of THz spectroscopy is that the transient electric field itself is measured, not simply its intensity, and this determines the amplitude and phase of each of the spectral components

10.1021/cr020685g CCC: $48.50 
Published on Web 03/09/2004

that make up the pulse. The amplitude and phase are directly related to the absorption coefficient and index of refraction of the sample, and thus, the complex-valued permittivity of the sample is obtained without having to carry out a Kramers−Kronig analysis. While there exist methods for determining the index of refraction when using conventional far-IR sources and detectors, it is noted that the great majority of the far-IR results reported in the literature present the frequency-dependent absorption coefficient, but not the refractive index. In this respect, THz spectroscopy provides a convenient method for determining the complex permittivity, even for studies that are not time-resolved. The allure of THz spectroscopy is easily understood: (1) It is a tabletop experiment with brightness equal to or exceeding that of synchrotron sources (at long wavelengths). (2) Coherent detection allows pulses below the blackbody radiation level to be measured without the use of specialized detectors. (3) Time-resolved studies are now possible in the far-IR region of the spectrum.

It is necessary to define the scope of this review and the time period covered. The scope of this review is experimental time-resolved THz spectroscopy. There has been far more work over the years involving spectroscopy in the THz region of the spectrum (often referred to as far-IR or submillimeter wave spectroscopy) which does *not* exploit the time-resolved and/or spectroscopic nature of this method, and is therefore beyond the scope of this review. In addition, as emphasized in section 2.14, THz time-domain spectroscopy (THz-TDS) does *not* measure dynamics; this terminology has caused some confusion. The measurement is made in the time domain, but only equilibrium properties of the sample are probed. The interested reader is directed to several reviews/overviews that have recently been published.[1−11] For example, THz imaging and sensing have seen a great deal of activity.[2] There has also been a surge of activity in biomedical imaging and cw spectroscopy of biological molecules. In fact, there have recently been two journal issues devoted to the biomedical and biological aspects of THz imaging and spectroscopy.[12,13]

THz spectroscopy grew out of efforts to generate and detect ultrashort electrical transients as they propagated down a transmission line. Research groups led by Dan Grischkowsky (then at IBM Watson Research Center) and David Auston and Martin Nuss (then at Bell Labs) were all active in this area. As understood from Maxwell's equations, a time-varying electric current will radiate an electromagnetic pulse. Thus, it was realized that these transmission lines were also radiating short bursts of electromagnetic radiation. A radical change occurred in 1988/1989 when reports were published wherein these radiated pulses were propagated through free space from a generator to a detector.[14,15] At this point, one could now envision using these elements as a far-IR light source and detector pair, and one could place a sample between the two of them. The defining factor is *free space propagation*. Earlier work involved propagation within crystals or along strip lines. While it is possible to carry out limited spectroscopic studies with these configurations, one needs free space propagation for a general spectrometer capable of characterizing solids, liquids, and gases. Thus, the time period covered in this review is from 1988 through the middle of 2003.

## 2. Experimental Considerations

This review focuses on the time-resolved experiments that are now possible with THz spectroscopy. However, a broad discussion of different types of sources and detectors will provide a better appreciation of this relatively new technique.

### 2.1. Photoconductive Antennas

Use of photoconductive antennas is the oldest method for generating and detecting THz pulses.[14−25] It is based on the process of using an above-bandgap laser pulse to generate carriers in the conduction band of a semiconductor under an applied bias voltage. The bias accelerates the newly formed carriers, yielding an electromagnetic pulse. This type of source can provide a bandwidth as high as 5 THz.[26] Because it is a resonant excitation method, it is limited not only by the excitation laser pulse width, but also the response time of the material. This type of source is typically used with oscillator-only, i.e., nonamplified, systems, and there has only been a small amount of time-resolved work using this type of THz pulse generator. The generation of THz pulses in photoconductive antennas has been modeled numerically[27−29] and analytically.[30]

A generic setup is shown in Figure 1.[31] The transmitter consists of a transmission line deposited lithographically onto an undoped GaAs wafer. The parallel metal strips of the transmission line are 1.6 cm in length and are separated by 30−60 $\mu$m. A dc bias voltage of 9−18 V is applied across the gap via wires bonded to pads at the end of each strip with indium metal. When a near-IR pulse from the Ti:sapphire illuminates the semiconductor surface between the metal strips, the acceleration of photoexcited electrons in the dc field radiates a femtosecond THz pulse, which is collimated by a crystalline quartz or silicon hyperhemispherical lens and an off-axis paraboloidal mirror. The dimensions of various parts of the antenna differ among all the groups who use this type of transmitter, but the numbers given here are broadly representative. Ralph and Grischkowsky studied the dependence of THz amplitude as a function of distance between the electrodes, and reported significantly higher pulse amplitude when photoexciting the semiconductor wafer near the anode.[18]

Several workers have employed low-temperature-grown GaAs (LT-GaAs) as the substrate for these THz emitters.[21−23] This material is produced using molecular beam epitaxy of GaAs at low substrate growth temperatures, $T_g = 180-300$ °C, in an excess As flux, followed by a high-temperature anneal, $T_a = 400-800$ °C, for a short period of time, $t_a = 1-30$ min. The resulting material has novel properties that differ from those of regular GaAs. Before annealing,

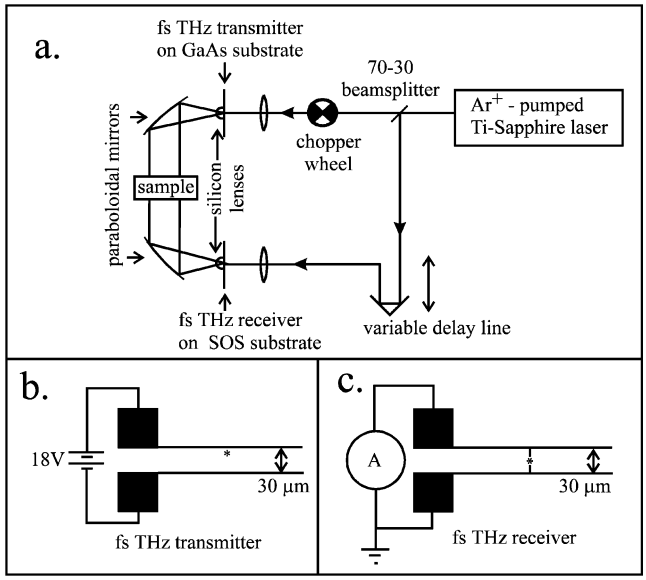


**Figure 1.** Schematic diagram of the THz-TDS spectrometer. A femtosecond THz pulse is generated at the transmitter when it is illuminated by a near-IR femtosecond pulse from the Ti:sapphire laser. After collimation by the lens and paraboloidal mirror, the femtosecond THz pulse passes through the sample and is refocused at the receiver. The receiver is gated synchronously by a portion of the beam split off from the near-IR pulse, so that the current flow at the receiver will map out the time-dependent electric field of the femtosecond THz pulse as the variable delay is adjusted. Panels b and c: Schematic diagram of femtosecond THz transmitter and receiver geometries. The asterisk represents the site at which the near-IR laser is focused. Reprinted with permission from ref 31. Copyright 1996 American Chemical Society.

the as-grown material is highly nonstoichiometric, containing excess As, and its properties are governed by point defects such as As interstitials and As antisites.[32] Photoexcitation of the as-grown material results in subpicosecond carrier lifetimes. Furthermore, the as-grown material is conductive in its nonphotoexcited state.[33] The material properties change dramatically upon annealing due to the precipitation of As clusters. The number of point defects is reduced as the excess As precipitates into clusters in an Ostwald ripening process.[32] The material can then be best described as a mixture of metallic As clusters embedded in a GaAs semiconductor matrix. The carrier trapping time in LT-GaAs is on a picosecond time scale,[34] unlike semi-insulating (SI) GaAs, which has carrier recombination times on the order of nanoseconds. The THz generation characteristics, such as amplitude and bandwidth, are not significantly better when using LT-GaAs than SI-GaAs; however, it has demonstrated notable advantages as a receiver material.

Terahertz antennas based on modulation of the current within superconducting $YBa_2Cu_3O_{7-\delta}$ thin films have also been investigated for use as a THz source, but to date have not performed as well as standard photoconductive antennas.[35−38]

The receiver consists of a transmission line bridged by an antenna with a gap in the center.[14−17,26,39,40] Its operation is similar to that of the transmitter, except that rather than applying a dc bias voltage, the transient THz field itself provides the bias voltage. If the gap is gated by the near-IR pulse when there is a large THz field, carriers will move from one side of the antenna to the other. The material used for the receiver is typically radiation-damaged silicon-on-sapphire or LT-GaAs, and has a very short carrier lifetime. Therefore, the electrons flow for roughly 100 fs, and after the THz pulse has passed and there is no longer a bias voltage, the electrons cannot travel back across the gap because the carriers have been trapped or have recombined due to their short lifetime. Instead, charge flows from ground through the picoammeter in proportion to the amplitude of the THz field at the moment when the near-IR pulse gated the receiver. The full waveform is mapped out by stepping the variable delay line incrementally. The sign of the field is determined in addition to its magnitude. Optimization of photoconductive antenna transmitters and receivers has been discussed by many authors.[14−17,26,39,40]

## 2.2. Planar Antennas

It is also possible to fabricate planar electrodes for THz pulse generation by depositing thin metal films or growing p−i−n diodes.[41−43] A p−i−n diode is comprised of an n-type semiconductor substrate with a ∼500 nm semi-insulating semiconductor material, followed by about 20 nm of p-type material, and an optional 5 nm of metal for a semitransparent electrode. Extremely high bias fields can be generated because the insulating layer is so thin. In fact, one of the largest bandwidth sources reported to date utilizes a p−i−n structure.[44] Also, it has been shown that it is possible to generate THz pulses by simply depositing a thin layer of metal film onto the GaAs wafer.[45,46] These types of sources are shown schematically in Figure 2. Because the applied bias voltage is along the surface normal, the wafer must be tilted to generate a usable signal. The back electrode is either a metal film or a highly doped semiconductor, and the THz radiation propagates in the direction of the specularly reflected beam. Other workers have shown that the surface depletion field present at the semiconductor/air interface can accelerate photogenerated carriers in the same manner as the THz planar emitters described above.[39,47−53] Because this type of transmitter does not have a metal electrode deposited onto it, a THz pulse is generated in both the forward and reflected directions. This process has also been investigated with Monte Carlo simulations.[54] It has been shown that the emission is enhanced at high temperatures, with a factor of 30 being obtained at 500 K.[55]

## 2.3. Magnetic Field Enhancement

Over the last five years significant effort has been directed toward enhancement of THz pulse generation from the surface depletion field in semiconductors using a static magnetic field of 1−7 T.[56−72] A schematic representation of a commonly used experimental setup is shown in Figure 3.[57] There are variants in which the magnetic field is not in the direction shown, and ref 61 compares a variety of orientations. Bolometric detection is usually used,

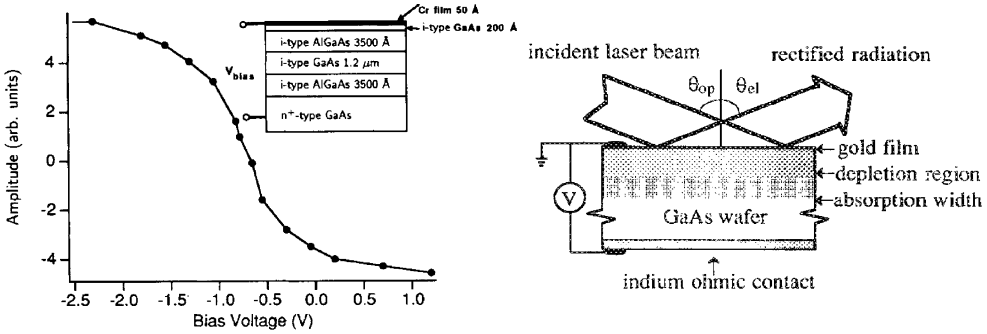


**Figure 2.** Left side: THz amplitude as a function of bias voltage on a p−i−n diode. The inset is a schematic representation of a p−i−n diode. Reprinted with permission from ref 43. Copyright 1994 American Institue of Physics. Right side: Schematic diagram of the planar emitter formed by depositing a gold film on a GaAs wafer. Reprinted with permission from ref 45. Copyright 1994 American Institute of Physics.

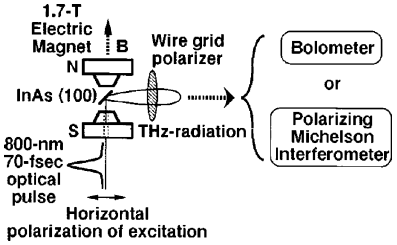


**Figure 3.** Schematic diagram of the configuration used to enhance THz emission with a static magnetic field. Reprinted with permission from ref 57. Copyright 1998 American Institute of Physics.

either with or without an interferometer, but sometimes photoconductive antenna receivers are used as well. Power enhancements of 1−2 orders of magnitude with magnetic fields on the order of 3 T are typically reported. Extremely high power levels have been reported—as high as 650 $\mu$W[57] (compared to roughly 10 nW from photoconductive antenna sources).[17] Oddly, the signal-to-noise ratio obtained in the power spectrum tends not to improve even as the overall THz power increases. Perhaps the noise is being enhanced as well as the signal.

The origin of the enhancement is now reasonably well understood.[64,73−75] The details of the theoretical treatments vary, but they all include the same elements. The photoexcited electrons are accelerated by the surface depletion field (ref 75 also considers the photo-Dember effect, wherein an electrical polarization can be photoinduced near the surface, due to the difference in mobilities between electrons and holes). Because the acceleration of charge is along the surface normal, no radiation is emitted in that direction. However, when there is a magnetic field perpendicular to the electric field, carriers are accelerated at right angles to their travel by the Lorentz force, thereby leading to a component of the acceleration in the surface plane. The other important issue is the angular dependence of the transmission coefficient of the THz pulse at the air/dielectric interface, given the fact that semiconductors have refractive indexes on the order of 3.5 in this region of the spectrum.

There have been variations on the magnetic enhancement theme. In one case a p−i−n planar diode was used to provide the electric field rather than depending on the depletion field.[76] A somewhat different approach has been to use an InAs crystal in a magnetic field as an intracavity saturable Bragg reflector in a mode-locked Ti:sapphire oscillator.[77−80]

## 2.4. Large-Aperture Antennas

When amplified lasers are employed for photoexcitation, it is impossible to use standard photoconductive antennas because the high pulse energies would destroy the material when focused down to spot sizes of a few tens of micrometers or less. Two solutions to this problem have been invoked: large-aperture photoconductive antennas and optical rectification.

As their name implies, large-aperture antennas have much wider separation between the two electrodes, thereby allowing a nonfocused excitation beam to be used to alleviate the potential for destroying the material.[81−85] The drawback is that a very high bias voltage is required. For example, 10 V applied over a 10 $\mu$m gap provides an average field of $10^4$ V/cm. On the other hand, if the electrode separation is 2 cm, then 20 kV is required to generate the same field (although many workers use only 1−2 kV/cm with large-aperture antennas). This presents some technical obstacles, but they can be overcome. The highest THz pulse energy reported to date (0.8 $\mu$J/pulse) was obtained using a large-aperture photoconductive antenna.[84] It is found that the emitted THz amplitude scales linearly with bias voltage and increases with increasing optical fluence, but saturates at levels higher than about 0.2 mJ/cm$^2$.[82,83]

Recently, a spectrometer based on a semi-large-aperture photoconducting antenna and nonamplified Ti:sapphire laser oscillator was reported.[86] The electrode spacing was 400 $\mu$m, and a square wave bias of ±400 V was used. A peak-to-baseline ratio of about 2000:1 was obtained when using a 1 mm thick ZnTe detector crystal and only 20 ms of scanning time.

## 2.5. Optical Rectification

A more popular choice for THz pulse generation when working with amplified lasers is to employ optical rectification in a nonlinear medium.[87−95] The material of choice has been ZnTe, although GaAs and GaP have been used as well. A typical setup is described in ref 96. It is based on a regeneratively amplified Ti:sapphire laser providing pulses at a 1 kHz repetition rate, with 100 fs pulse duration and

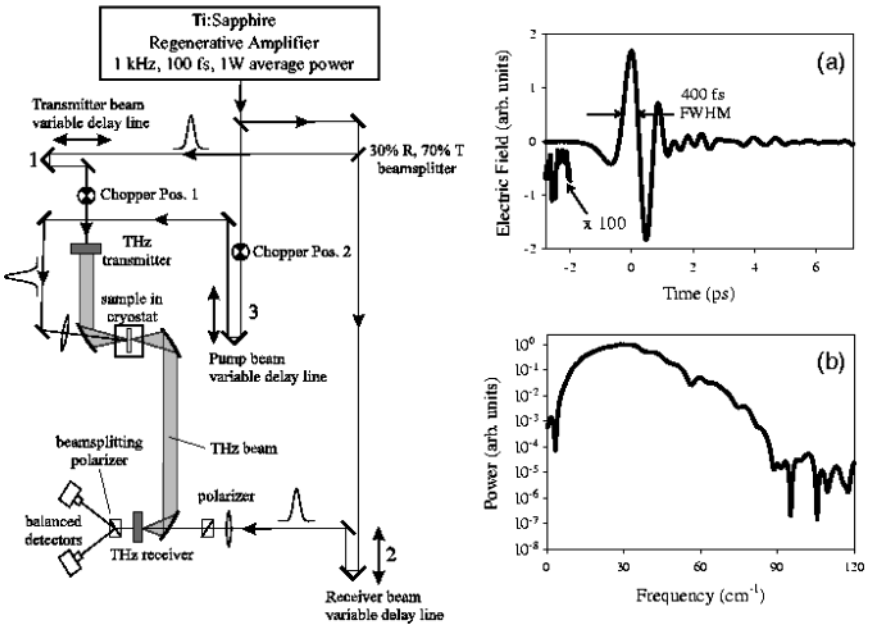


**Figure 4.** Experimental apparatus used to collect TRTS spectra. A reference scan is collected with the chopper in position 1, and a photoexcited difference scan is collected with the chopper in position 2. The THz amplitude is monitored by changing the relative delay of table 1 or table 2 depending on the type of experiment being performed (see the text for more details). Delay table 3 is used to change the relative delay of the pump beam. (a) shows a typical time-domain THz transient of about 400 fs duration (fwhm) and signal-to-noise ratio of roughly 1000:1. (b) shows the power spectrum of the THz pulse. Reprinted with permission from ref 96. Copyright 2000 American Institute of Physics.

1 mJ/pulse energy, at 800 nm wavelength, and is shown schematically in Figure 4, along with the time-domain THz amplitude and frequency-domain power spectrum.

Optical rectification is the difference frequency analogue of second harmonic generation. That is, when light interacts with a nonlinear medium and wave mixing between two frequencies, $\omega_1$ and $\omega_2$, occurs, the result is sum-frequency generation, $\omega_1 + \omega_2$, and difference-frequency generation, $\omega_1 - \omega_2$. In the case where $\omega_1 = \omega_2$, one generates both second harmonic and dc pulses. Because the near-IR pulse has a duration of ~100 fs, a "dc" pulse corresponding to the envelope of the optical pulse is generated rather than a constant dc level. Alternatively, this generation mechanism can be understood by considering the fact that the optical pulses have significant bandwidths. Thus, the high-frequency components can mix with the low-frequency components within a given pulse to produce a pulse at the difference frequency. Since the optical pulses have a bandwidth of a few THz, the difference frequencies fall in the THz range.

One advantage of optical rectification is that it is a nonresonant method and the THz pulse width is limited only by the optical laser pulse width (and the phonon-mode absorptions of the crystal), and not the response time of the material. Some of the shortest THz pulses to date, displaying bandwidths up to 100 THz, have been generated in this or a similar fashion (see below).[95,97−99]

It has also been shown that organic molecular crystals are capable of generating THz pulses via optical rectification.[100−102] One popular choice has been the organic ionic salt 4-*N*,*N*-dimethylamino-4′-*N*′-methylstilbazolium tosylate (DAST),[101] but (−)-2-(α-methylbenzylamino)-5-nitropyridine (MBANP) has also been shown to work well,[102] as have multilayered polymer films.[100] These materials are more efficient than ZnTe crystals of the same thickness, but have not yet found widespread use.

## 2.6. Free Space Electrooptic Sampling

When using an amplified laser system, the pulses are best detected via free space electrooptic sampling (FSEOS) rather than with photoconductive antennas.[96,97] This has the advantage that it is a nonresonant method of detection, so the potential for damaging the detector crystal with the focused readout beam is much lower. It is also possible to obtain a two-dimensional THz image without raster-scanning the object by using a large electrooptic crystal (25 mm × 25 mm) and a CCD camera detector.[103,104] However, there are far more examples of workers using optical rectification/FSEOS with unamplified laser systems,[44,91,92,94,95,99,105−107] or perhaps a semi-large-aperture antenna as a generator and detecting with optical rectification with an unamplified Ti:sapphire oscillator.[86] Issues related to copropagation of the readout beam and THz beam and other sources of distortion of the measured pulse have been treated theoretically.[87,108−111]

The THz radiation is typically detected by FSEOS in a 0.5−1.0 mm thick ⟨110⟩ ZnTe crystal, although for high-bandwidth applications it must be as thin as 10 μm. It is based on the Pockels effect in which an applied voltage causes the detector crystal to become birefringent. When the optical sampling pulse travels through the crystal at the same time as one point in the THz pulse, its polarization is slightly rotated. The magnitude of rotation is proportional to the magnitude of the THz field, and the direction of rotation is proportional to the sign of the field. In this

manner, the entire pulse amplitude as a function of time is mapped out by scanning the delay line that determines when the readout pulse arrives at the detector crystal relative to the THz pulse. The signal is collected with a lock-in amplifier phase-locked to an optical chopper, which modulates either the THz generation arm or the pump beam (when a pump−probe experiment is performed). The THz beam path from the transmitter to the receiver is usually enclosed and purged with dry nitrogen to minimize THz absorption by water vapor.

## 2.7. Single-Shot Detection

There are situations when single-shot detection is desirable, such as when a high-power low-repetition-rate experiment or a destructive experiment is being performed. It is possible to collect an entire THz waveform without having to scan a delay line. This is usually performed by chirping the optical readout beam prior to sending it through the electrooptic crystal, and using a monochromator with a CCD camera detector to detect the different spectral components of the chirped pulse which correspond to different points on the time axis.[112−115] It is also possible to perform single-shot detection by propagating the readout beam through the electrooptic crystal at an angle relative to the propagation direction of the THz beam.[116] In this manner, different spatial portions of the readout beam will sample the THz pulse at different times. Finally, it is possible to perform single-shot detection over a linear spatial range, leading to a two-dimensional (2D) data set with time as one axis and position as the other.[112] In this case, a chirped readout beam is used, and it is focused to a line using a cylindrical lens. It is then dispersed perpendicular to this direction by a monochromator fitted with a CCD camera. Thus, the spatial dimension is obtained directly, and the time delay is obtained by using a chirped pulse.

## 2.8. High-Bandwidth Sources

One area of interest in the THz community has been to increase the bandwidth and spectral coverage (at the expense of the signal-to-noise ratio).[44,95,97,99,117,118] Zhang and co-workers reported pulses with spectral coverage to 37 THz using a 10 $\mu$m thick GaAs transmitter and 10 $\mu$m thick ZnTe receiver.[95] Leitenstorfer et al. utilized a p−i−n diode to generate tunable THz radiation over a range of 2 to about 60 THz,[44] although in both of these cases there are gaps in the spectrum due to phonon modes of the transmitter and/or receiver. It is also possible to employ phase-matched difference-frequency mixing in GaSe (30−100 $\mu$m thickness) to generate bandwidths up to 40 THz.[97,99,117] Electrooptic sampling is typically used in high-bandwidth applications, but there are notable exceptions.[119−122] In fact, Kono et al. reported bandwidths out to 60 THz when gating the photoconductive antenna with 15 fs laser pulses.[119]

## 2.9. Synchrotrons and Free Electron Lasers

Synchrotrons and free electron lasers can generate short pulses of far-infrared radiation, typically on the order of 5−10 ps (although latest-generation FELs can produce subpicosecond pulses). While these sources are quite different from all the other THz sources considered here, they have in fact been employed in time-resolved measurements over the years (although with lower temporal resolution than the other work reported here), which warrants their mention. An obvious disadvantage to this type of source is their high cost and therefore limited availability and accessibility. These sources will not be further considered in this review, but their advantages of broad tunability and high power levels, especially at higher frequencies, are noted.

## 2.10. Lithium Niobate

Two methods for THz generation are based on $LiNbO_3$. One employs parametric oscillation in a lithium niobate crystal, using either a grating coupler or a Si prism coupler,[10,123−130] and the other employs periodically poled lithium niobate as a nonlinear medium to downconvert visible pulses to narrowband radiation in the THz region.[131−133] These transmitters have some intriguing aspects, but their power levels are not as high as those in more traditional methods. Furthermore, the pulse durations tend to be on the order of 100 ps to about 1 ns (which leads to high spectral resolution). These sources will find more use in studies that do not involve dynamics, and will not be considered further.

## 2.11. Laser-Generated Plasmas

It has been shown that laser-generated plasmas can produce radiation up to 4 THz.[134−137] The THz pulse can be generated via ponderamotive acceleration of electrons by the intense laser pulse,[134,135] or by an applied bias voltage across an air gap in a manner similar to that of photoconductive antennas,[136] or by nonlinear four-wave mixing of the fundamental and second harmonic frequencies of the laser beam in air or a variety of gases.[137] A potential advantage for this type of source is that there will not be absorptions from phonon modes of the transmitter material. While they have not yet found widespread use, they show great promise.

## 2.12. Transceivers

There have been some notable recent developments in using a single structure for both the transmitter and receiver—i.e., a transceiver.[138−140] Transceivers based on both photoconductive antennas and electrooptic crystals have been demonstrated. However, the advantages of this sort of arrangement are realized in THz sensing and ranging studies rather than spectroscopic ones. It is worth mentioning them in the event that they become more readily available, achieve a higher signal-to-noise ratio, or become easier to use soon and are adopted for time-resolved spectroscopy studies.

## 2.13. Other Methods

Photoconductive antennas and FSEOS remain the workhorses of THz detection techniques, but other

methods do exist. Interferometric characterization of the spectral properties of THz pulses has been demonstrated.[48,141−143] This is typically achieved by using a beam splitter to divide the pulse into two equal portions in the interferometer;[48,141,142] however, it is also possible to employ two identical THz sources and make them interfere with each other.[143] Nahata and Heinz demonstrated that it is possible to detect THz pulses via optical second harmonic generation.[144] The presence of the THz electric field modifies the amount of second harmonic generation at a silicon surface. Bromage et al. showed that dithered edge sampling provides a means to achieve improved bandwidths from photoconductive antennas, at the expense of a slightly more complicated setup.[145] Polarization modulation, as opposed to amplitude modulation, when using optoelectronic detection has also been demonstrated.[89]

## 2.14. THz Time-Domain Spectroscopy

THz-TDS has become a widely used technique, and the great majority of THz studies have employed this method. However, even though the measurement is made in the time domain, it is not a time-resolved technique. It is equivalent to a Fourier transform far-infrared method, and does not provide time-resolved dynamical information. It has several notable advantages relative to other methods in the far-IR, such as broad coverage, determination of both absorption coefficient and refractive index, and coherent synchronous detection that is immune to ambient blackbody radiation. However, because this review is concerned with dynamics, THz-TDS will not be considered further. The interested reader is directed toward refs 1 and 2 as a place to begin.

# 3. Time-Resolved THz Spectroscopy

The remainder of this review will consider several time-resolved methods that characterize dynamics. There exist several broad categories: (1) experiments that involve the generation of a THz pulse to understand some dynamical event (as opposed to creating a better THz source), (2) experiments in which the average far-IR response of the material is probed as a function of time after photoexcitation of the sample, (3) experiments in which the entire THz waveform is obtained at a certain amount of time after photoexcitation of the sample, and (4) two-dimensional studies in which the entire THz waveform is obtained at a variety of times after photoexcitation to map out the evolution of the far-IR spectrum, and thereby provide a connection to the underlying photoinduced changes in the medium.

## 3.1. THz Emission Spectroscopy

The majority of time-resolved THz experiments fall into the category of THz emission spectroscopy. In general, a sample is photoexcited and radiates a THz pulse due to a change in current and/or a change in polarization in the sample, and the radiated THz waveform is analyzed to uncover the dynamics of the underlying process. This section is broken down into four subsections: (1) bulk semiconductors, (2) semiconductor quantum wells and superlattices, (3) superconductors, (4) other materials.

### 3.1.1. Bulk Semiconductors

The analysis of THz pulses emitted from semiconductors can be used to learn about the carrier dynamics of the materials themselves.[29,146,147] This type of study has been carried out for GaAs under different applied bias voltages,[148,149] at a variety of temperatures,[150] and as a function of magnetic field.[57]

There has been a small amount of work utilizing photoconductive antenna geometries. For example, the temperature-dependent output, which depends on the momentum relaxation time, has been characterized at cryogenic temperatures,[150] as has the dependence on bias voltage and excitation power, which vary with carrier acceleration and velocity overshoot and screening, respectively.[21] The carrier lifetime and mobility in $O^+$ ion implanted 300 nm thick amorphous Ge films were found to be as short as 600 fs and roughly 100 $cm^2\ V^{-1}\ s^{-1}$, respectively.[151]

Somewhat more work on dynamics has been carried out using THz emission from semiconductor surfaces utilizing the surface depletion field rather than an applied bias voltage. The temperature dependence of the radiation from an InP surface has allowed the contribution from acceleration in the surface field to be separated from that due to the photo-Dember effect. In fact, the polarity of the pulse reverses below 120 K.[152,153] It is also possible to monitor the surface field directly using transmission electrooptic sampling, and compare the results with the emitted waveform.[51] A biased metal film on the surface can control the surface depletion field, which allows the dependence of the carrier dynamics on the surface field to be explicitly measured.[45] The temperature dependence of the carrier scattering times in GaAs at temperatures up to 900 K has been measured.[55] A 6-fold enhancement of the THz power at 500 K is attributed to impact ionization, which amplifies the number of carriers participating in the transient current. At higher temperatures, there is significant scattering into the low-mobility L valley, leading to a loss in THz emission. A comparison of InAs and InSb led to the conclusion that the photo-Dember effect was the mechanism responsible for THz generation in these semiconductors.[53] The cryogenic temperature dependence of these two semiconductors was investigated, which further supported the conclusion that the photo-Dember effect is responsible for THz generation in these materials.[52]

The study of carrier dynamics in p−i−n diodes was first carried out in the early 1990s. By varying the applied bias voltage and tuning the excitation wavelength across the band edge, the effects of displacement and transport current were separated, as well as observation of velocity overshoot in GaAs.[41,43,154] It is also possible to use the internal field of a p−i−n diode to create plasma oscillations.[155] The dynamics can be varied by changing the carrier density. By using 12 fs optical pulses, and an extremely thin ZnTe detector crystal (∼10 $\mu$m), Leitenstorfer et al. obtained a detailed picture of the transport dynamics in very large electric fields (up to 130 kV/cm).[148,149,156]

### *3.1.2. Semiconductor Heterostructures*

THz emission studies have been carried out to understand dynamics in systems ranging from a single heterojunction interface, to single, double, and triple coupled quantum wells, to superlattices and microcavities. All of these structures are based on layers grown with user-defined thicknesses of dissimilar semiconductors, one of which has a larger band gap than the other. There are issues of lattice mismatch and strain at the interface. The ternary compound $Al_xGa_{1-x}As$ is often chosen in conjunction with GaAs because the lattice constants of AlAs and GaAs are almost identical. The room temperature band gaps of GaAs and AlAs are 1.43 and 2.15 eV, respectively,[157] and the band gap of $Al_xGa_{1-x}As$ lies between these values, depending on the stoichiometry. Figure 5 shows schematic representations of a variety of heterostructures.

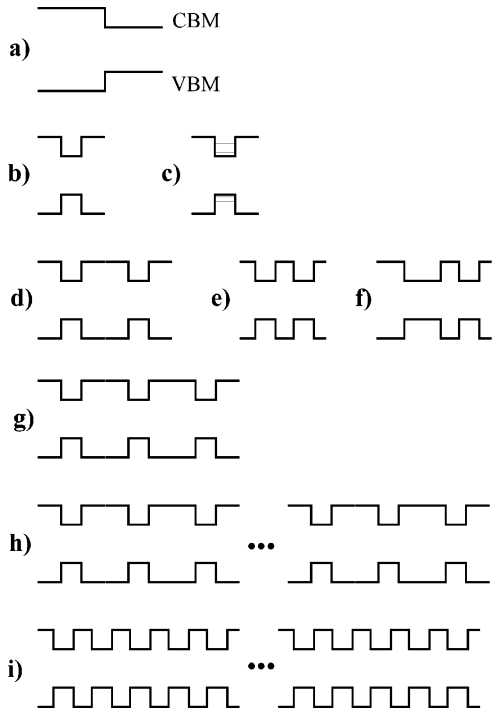


**Figure 5.** A variety of heterostructures. The conduction band minimum is denoted CBM and the valance band maximum VBM. (a) is a heterojunction, (b) is a single QW, (c) shows its energy levels, (d) is a double QW, (e) is a coupled double QW, (f) is an asymmetric coupled double QW, (g) is a triple QW, (h) is a multiple QW, and (i) is a superlattice.

A heterojunction is simply the interface between two dissimilar materials. The next step in complexity is a single quantum well (QW), which is obtained when the thickness of the small-band-gap material is on the order of 50−150 Å and is sandwiched between layers of the large-band-gap material. This causes quantum confinement along the growth dimension, leading to discrete energy levels. The energy levels are more widely separated as the well thickness is decreased. The wave functions associated with these energy levels (not shown in Figure 5) "leak out" beyond the interface because the confinement potential is not infinitely high. A double QW is simply two single QWs deposited onto a substrate. A coupled double QW is achieved when the separation between the two single QWs is small enough that the wave functions overlap with each other, which is usually on the order of 10−30 Å. An asymmetric coupled double quantum well has two QWs of differing widths, and therefore different energy level spacings, that are coupled to each other (under the proper bias voltage). A triple QW is simply three single QWs, and a multiple QW is an arbitrary number of single QWs. A superlattice is an arbitrary number of *coupled* QWs, which leads to the formation of minibands.

Using a grating coupler, Hirakawa et al. characterized the decay rate of 2D plasmons at a single $Al_{0.3}Ga_{0.7}As/GaAs$ heterojunction by carrying out THz emission experiments at a variety of temperatures and excitation wavelengths (near and above the band gap).[158] Later, they employed $\delta$-doped single QWs to spatially confine the carriers, which does not occur at a single interface, and observed THz emission from up to fifth-order 2D plasmon modes.[159−161]

In 1992 Planken et al. used a multiple QW of uncoupled single QWs to demonstrate that a field-induced polarization of electron−hole pairs produces a THz pulse, thereby proving that current transport is not necessary.[162,163] At low temperatures, the barriers of the single quantum well confine electrons and holes even in the presence of a bias voltage. However, the bias field will polarize the newly created electron and hole wave functions, thereby leading to a THz pulse. Later, they showed that THz emission could be produced from both uncorrelated $e-h^+$ pairs and polarized excitons which could be coherently excited and controlled.[164,165] Schaff and co-workers monitored parallel transport within QWs (i.e., within the plane of the QWs), and found many of the same phenomena as for bulk material, such as ballistic acceleration on a time scale of 150 fs, saturation of carrier velocity on a 1 ps time scale, and energy overshoot.[166]

Coupled asymmetric QWs have also received much attention.[167−173] These differ from single QWs in that the THz emission from a single QW under a bias voltage is due to polarization of the electron and hole wave functions, whereas in a coupled asymmetric quantum well, the bias voltage brings the electronic energy levels into resonance, causing a splitting. However, the hole energy levels are not brought into resonance (see Figure 6a).[167] Thus, when the coupled energy levels are excited, the electrons oscillate back and forth between the wells, but not the holes, leading to a time-dependent polarization at the tunneling frequency. Observation of THz emission due to coherent oscillations between the two wells was observed in 1992,[167] and controlled in 1993.[168] The emitted waveform in the work published in 1992 is shown in Figure 6b.[167] The energy levels in the narrow well and wide well are brought into resonance with a 10.5 kV/cm bias voltage. It was expected that the frequency of the oscillation persisting for 5 ps after the primary feature would depend parabolically on the difference between the applied field and 10.5 kV/cm, but it did not. The fact that the frequency was essentially independent of bias voltage is due to excitonic interactions between the holes and electrons

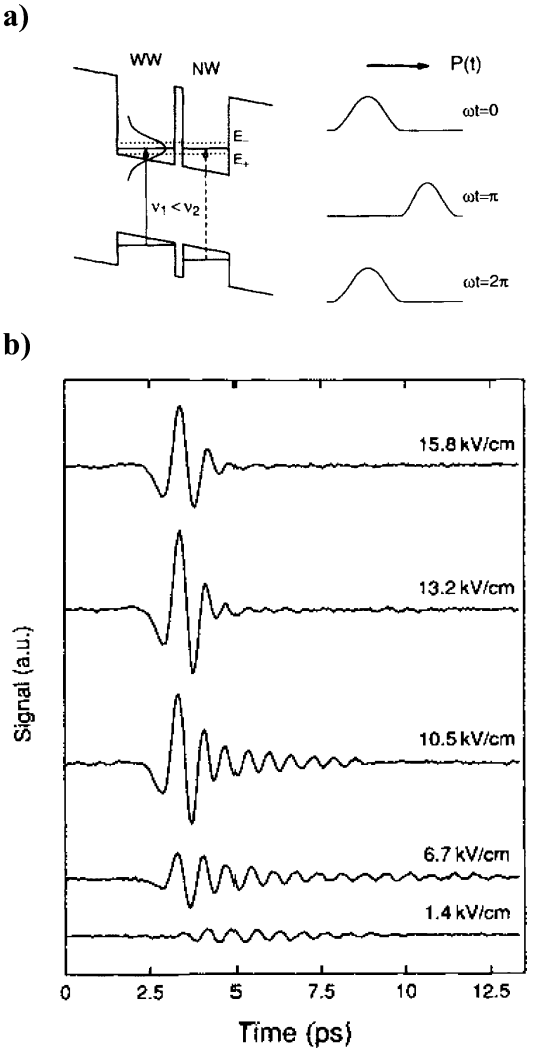


**Figure 6.** (a) is a diagram of an asymmetric double quantum well. When the electron levels are brought into resonance, charge can oscillate back and forth as depicted on the right. (b) shows the THz emission obtained at several bias voltages. The electron levels are resonant at 10.5 kV/cm. Reprinted with permission from ref 167. Copyright 1992 American Institute of Physics.

in the two wells, as well as the presence of light holes and heavy holes which are not shown in the simple schematic diagram of Figure 6a.[167] Theory and experiment are in good agreement.[169,170,173] As the temperature is lowered, the coherence lasts longer, and the THz emission decays more slowly. More recent efforts have also shown this phenomenon, and characterized the excitation wavelength dependence of the THz signal due to instantaneous polarization within wells and tunneling between wells.[171]

Wave packet dynamics in symmetric, coupled triple QWs and quantum wires have also been recently characterized.[172,174] A theoretical treatment of coupled QWs using the exciton representation was reported in 1999. They discussed and compared disorder and phonon-induced dephasing effects.[175]

The first report of THz emission from a semiconductor superlattice appeared in 1990.[45] The strain-generated electric field in a ⟨111⟩ GaSb/AlSb superlattice produced a THz pulse upon optical excitation. Later, other workers applied a bias voltage to $Al_xGa_{1-x}As/GaAs$ superlattices and directly observed Bloch oscillations.[176−182] An unbiased superlattice forms minibands due to the periodicity of the lattice. When a bias voltage is applied, the band splits into a series of equally spaced states, with energy spacing $\Delta E = eFd$, where $e$ is the electron charge, $F$ is the field strength, and $d$ is the period of the superlattice.[183] This is known as a Wannier−Stark ladder (WSL). The accompanying oscillation of electrons among the coupled wells is known as a Bloch oscillation. The oscillation period associated with this energy splitting is of course $\tau_B = h/eFD$, where $h$ is Planck's constant. If the excitation pulse is tuned above or below the center of the WSL using a short pulse whose bandwidth spans several energy levels, then the center-of-charge also oscillates as the photoexcited electrons undergo harmonic oscillation,[183] which leads to THz emission (if $\Delta E/h$ is in the THz region of the spectrum). This is not unlike the phenomenon of coherent molecular vibrational motion initiated by a short excitation pulse whose bandwidth spans several vibrational quanta. It is the superposition of several stationary states that leads to coherent motion in both cases. In a series of papers during the mid-1990s, Kurz and Köhler and co-workers utilized degenerate four-wave mixing, THz emission, and transmission electrooptic sampling to unequivocally demonstrate Bloch oscillations in an $Al_xGa_{1-x}As/GaAs$ semiconductor superlattice.[176−180] This led to generation of superradiant emission from Bloch oscillations in an $Al_xGa_{1-x}As/GaAs$ superlattice. Shimada and co-workers also observed the crossover from miniband transport to the formation of a Wannier−Stark ladder in the photocurrent spectrum, with the concomitant THz emission from the Bloch oscillations.[181,182,184]

Yamanishi and co-workers utilized THz emission spectroscopy to characterize semiconductor microcavities.[185,186] Observation of emitted electromagnetic radiation proved that the exciton population is oscillating. They also found that the exciton dephasing time was independent of temperature below 50 K, indicating that the dephasing was due to sample inhomogeneity, and not phonon scattering.

It is possible to excite the sample with a THz pulse rather than optically.[187−190] For example, Nurmikko and co-workers observed electron cyclotron oscillations in heterostructures. In the case of an $Al_{0.7}Ga_{0.3}As/GaAs$ multiple QW, they compared the radiation emitted parallel and perpendicular to the incident polarization as a function of magnetic field.[187] They later studied a single modulation-doped heterojunction with a semitransparent electrode, which allowed them to depopulate the QW. They determined the electron dephasing time in a fixed 3.1 T magnetic field as a function of temperature. The dephasing time decreased from 2.8 to 0.7 ps as the sample temperature was increased from 2 to 150 K.[188] Kersting et al. fabricated $Al_{0.3}Ga_{0.7}As/GaAs$ heterostructures containing a QW with a parabolically shaped conduction band. This leads to equally spaced energy levels whose separation depends on the width of the QWs. These experiments involved exciting the intersubband transitions with a THz pulse, and mea-

suring the free-induction decay of the emitted THz pulse. By modeling the data with a density matrix formalism for a two-level system, they extracted the time-dependent population in the upper level.[189,190]

### 3.1.3. Superconductors

Terahertz emission from high-$T_c$ superconductors (HTSCs), particularly $YBa_2Cu_3O_{7-\delta}$ (YBCO), has also been a topic of considerable attention.[24,191−209] It is possible to characterize the dynamics of Cooper pair breaking and recombination. Also, HTSCs show promise as high-speed optical detectors, and understanding the relaxation of photoexcited quasiparticles is required. Hangyo and Tonouchi and their co-workers have been particularly active in this field. Terahertz emission from a superconducting sample was reported in 1996 and 1997.[191−196,199−201] Jaekel et al. characterized the temperature dependence,[194,195] while Tonouchi et al. concentrated on the excitation power dependence and bias current dependence, in addition to the temperature dependence.[191,193,196,199−201] The supercurrent is given as $j_s = eN_s(T)v$, where $e$ is the electron charge, $N_s(T)$ is the Cooper pair density, $T$ is the temperature in kelvin, and $v$ is the carrier velocity. Given that the radiated THz pulse is due to a time-dependent current, $E(t) \propto dj_s/dt$, both sets of authors attributed the pulse generated to a time-dependent change in Cooper pair density, $dN_s(T)/dt$. Tonouchi et al. also included the contribution of the change in carrier velocity to the change in supercurrent: $dv/dt$. Models based on these assumptions led to agreement in the trends observed as the temperature, excitation power, and bias current were varied. Later Tonouchi et al. carried out a temperature-dependence study and quantified the quasiparticle recombination time.[192,199,200] They found that the recombination time increased from about 0.3 ps at 10 K to about 2 ps at 70 K. Their results are not directly comparable to those of Jaekel and co-workers because Jaekel et al. carried out their analysis in the frequency domain, while Tonouchi et al. worked in the time domain. These results have recently been largely confirmed by Lin et al. using a detector based on FSEOS rather than a photoconductive antenna.[24]

Tonouchi et al. also investigated flux-trapping in YBCO thin films.[197,198] To carry out these experiments, they utilized a cylindrical magnet in close proximity to the superconducting film to provide a magnetic field of ∼150 G perpendicular to the surface normal (see Figure 7)[197] rather than a bias current.The sample is cooled to 11 K in the absence of a magnetic field. Upon photoexcitation a THz pulse is not generated in the absence of a magnetic field (see Figure 8),[197] but a THz pulse *is*

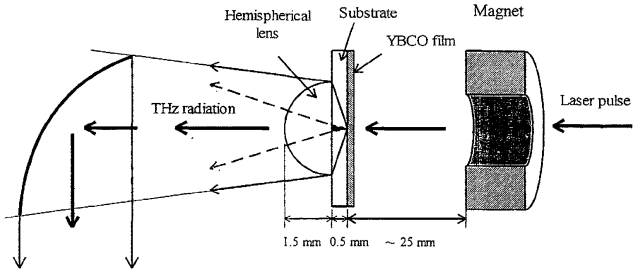


**Figure 7.** A cylindrical magnet provides the shielding current in a superconducting thin film. Reprinted with permission from ref 197. Copyright 1997 Publication Board, *Japanese Journal of Applied Physics*.

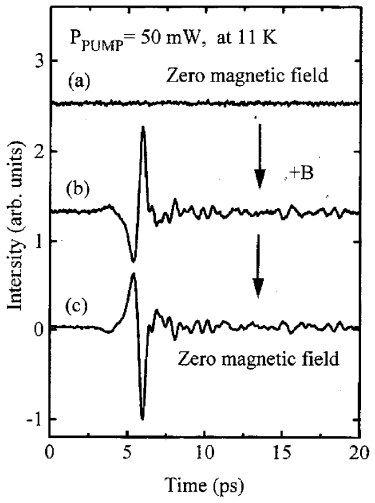


**Figure 8.** (a) displays the absence of THz emission after the sample is cooled, but before a magnetic field is applied. (b) displays THz emission in the presence of an applied magnetic field. (c) displays THz emission after the field has been removed. Reprinted with permission from ref 197. Copyright 1997 Publication Board, *Japanese Journal of Applied Physics*.

generated when a magnetic field is applied, and persists (with a polarity reversal) after the magnet is moved away. On the basis of the reversal of polarity, these results were interpreted as being due to modulation of the shielding current when the external magnetic field is present, and modulation of the supercurrent circulating around the trapped magnetic fluxes in the film after the magnet has been removed.[197,198]

More recently, Tonouchi and co-workers have characterized the THz emission from a YBCO superconducting thin film containing a Josephson junction.[204] They concluded that the THz emission properties were quite similar to those for standard YBCO antennas without Josephson junctions because the grain boundary occupies only a very small fraction of the area illuminated by the excitation laser.

Finally, there has been a small amount of work employing THz emission spectroscopy to investigate other thin film superconductors such as $Y_{0.7}Pr_{0.3}Ba_2Cu_3O_7$ (YPBCO),[203] $Tl_2Ba_2CaCu_2O_{8+\delta}$ (TBCCO) in a magnetic field,[209,210] and $YBa_2Cu_3O_{7-\delta}/PrBa_2Cu_3O_7$ (YBCO/PBCO) multilayers.[208] It was found that the THz amplitude emitted from the YPBCO sample was about 5 times larger than that from YBCO under identical conditions.[203] The THz emission from the TBCCO sample depended on the excitation intensity and temperature, and the results were consistent with the signal being due to supercurrent modulation of the Josephson plasma resonance.[209,210] The results from the multilayer samples indicate that the recombination dynamics do not change as the amount of PBCO relative to YBCO is changed, but that the signal amplitude can be significantly higher.[208]

### 3.1.4. THz Generation from Other Materials

There have been some interesting reports of THz emission from photoexcited samples that do not fall into the above categories. There has recently been work wherein oriented dye molecules are photoexcited in the THz pulse generated due the process of intramolecular charge transfer. The molecules have been either oriented with an applied static electric field[211,212] or grown as a crystal.[102,213] While the HOMO to LUMO electronic transition is essentially instantaneous, the change in polarization, which is responsible for THz pulse generation, is influenced by the surrounding medium. Results for the dye molecules betaine-30 [2,6-diphenyl-4-(2,4,6-triphenylpyridinio)phenolate] and DMANS [4-(dimethylamino)-4′-nitrostilbene], whose structures are shown in Figure 9, are shown in Figure 10. It is seen that the

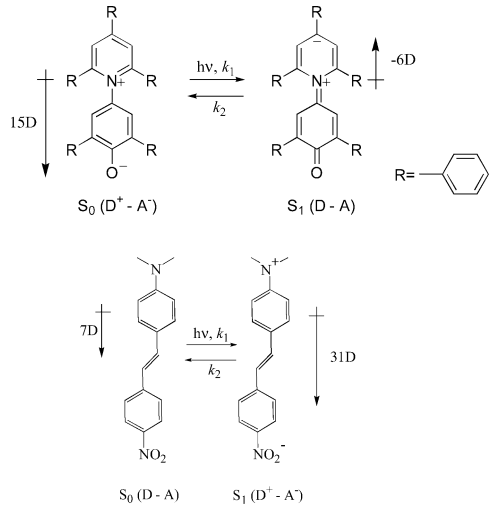


**Figure 9.** Ground, $S_0$, and first excited states, $S_1$, of betaine-30 (top) and DMANS (bottom) and their respective dipole moments. Reprinted with permission from ref 212. Copyright 2002 American Chemical Society.

polarity of the pulse is a direct measure of the direction of charge transfer relative to the ground-state dipole. The details of the shape of the pulse provide information on the time scale of the change in polarization. Beard et al. found that the solvent response time of chloroform is 350 fs, and that for toluene is 730 fs.[212]

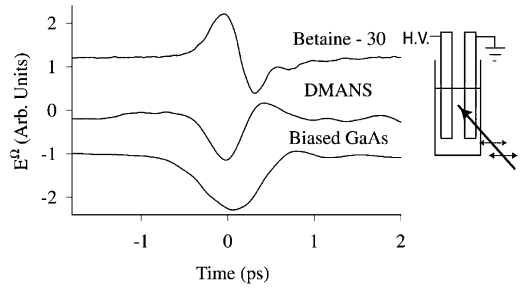


**Figure 10.** Electric fields generated via charge transfer in DMANS and betaine-30 compared to that generated from photoexcitation of biased GaAs. The applied voltage is in the same direction for all three samples. A schematic representation of the cuvette and electrodes is shown to the right. Reprinted with permission from ref 212. Copyright 2002 American Chemical Society.

Magnetoresistive manganite thin films of $Pr_{0.7}Ca_{0.3}MnO_3$ undergo an insulator to metal transition upon illumination in an applied electric bias field.[214,215] By making measurements at a variety of temperatures, Kida et al. were able to identify the transitions between charge ordering and orbital ordering, collinear antiferromagnetic ordering, and charge−orbital-ordered spin-canted antiferromagnetic insulating behavior.

A recent development in terahertz emission spectroscopy is concerned with the relativistic electron beam bunch diagnostics in accelerators and free electron lasers.[216,217] Not surprisingly, when an electron beam passes near an aperture, a THz pulse is emitted whose characteristics reflect the properties of the electron bunch. It is a nondestructive single-shot method, with subpicosecond temporal resolution.

### 3.1.5. Correlation Studies

There have been several correlation studies in which two optical pulses are used to photoexcite a biased semiconductor, and the resulting THz emission is measured as a function of delay between two excitation pulses.[146,205−207,218−224] A typical experimental configuration is shown in Figure 11.[220] These stu-

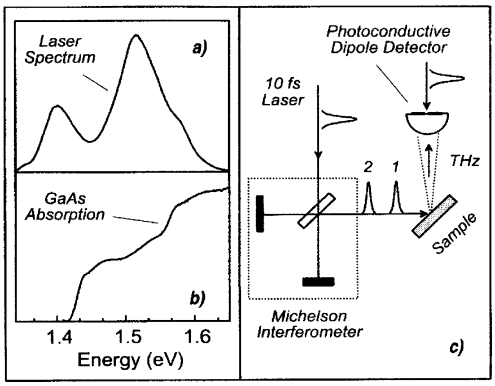


**Figure 11.** Generic setup for carrying out correlation studies. Reprinted with permission from ref 220. Copyright 1995American Institute of Physics.

dies are sometimes referred to as “pump and probe measurements”, but they are not pump/probe studies in the usual sense because the “probe” beam is not monitored directly, only its influence on the photocurrent or THz pulse that is generated.

The initial report by Keiding and co-workers in 1993 investigated carrier transport and screening in semi-insulating GaAs, and found that the local field is screened in less than 1 ps for high injected carrier densities ($1 \times 10^{18}$ $cm^{-3}$).[218] A subsequent paper in 1994 investigated photocurrent dynamics in ion-implanted silicon-on-sapphire.[219] It is known that this material has a short-lived carrier lifetime, and indeed they found that the photocarriers decayed in less than 1 ps. Furthermore, they also identified screening due to carriers trapped in long-lived trap states. In 1995, Nuss and co-workers carried out a very high time resolution study (10 fs temporal resolution), and identified the distinct phases of carrier transport in GaAs and Si.[220] They found that, upon photoexcitation, ballistic transport occurs within the first 70 fs, followed by electron velocity overshoot, which then

leads into steady-state drift within about 200 fs after photoexcitation. Similar studies were carried out for large-aperture GaAs photoconductive antennas in 1997.[221] They found that the screening in large-aperture emitters is smaller and occurs on longer time scales than that for small-aperture antennas. Tonouchi et al. found that LT-GaAs displays three scattering processes upon photoexcitation, which decay with time constants of 0.26, 0.85, and 1.25 ps.[224]

Huggard et al. investigated cyclotron emission from a 2D electron gas within two $Al_{0.3}Ga_{0.7}As/GaAs$ quantum wells.[222] They were able to enhance or diminish the cyclotron emission as a function of time between the first and second optical pulses. In particular, the emission was enhanced when the second pulse arrived after an amount of time corresponding to $2n\pi$ phase cycles, whereas it was nearly canceled out when the second pulse arrived after $(2n + 1)\pi$ phase cycles, where $n$ is an integer.

Coherent plasma oscillations in p−i−n and n-doped GaAs structures have been observed by Kersting et al.[155,223] They measured the integrated THz power as a function of time delay between two optical pulses using bolometric detection. The power spectrum emitted from the p−i−n structure depends on excitation densities, and that for the n-GaAs sample depends on the doping level. The spectrum shifts to higher frequencies at higher excitation densities for the p−i−n structure, and for higher doping levels for the n-GaAs samples.

More recently, this technique has been used to investigate carrier dynamics in current-biased superconducting YBCO thin films.[205−207] They investigated bias-current dependence, pump power dependence, and temperature dependence, and interpreted their results in terms of Cooper pair breaking, supercurrent modulation, and Cooper pair recombination.

#### 3.1.6. Tunable Narrow-Band THz Radiation

Tunable narrow-band THz radiation was originally observed using an experimental setup similar to that used for the correlation studies.[225,226] Given that it is narrow-band, the pulse durations are significantly longer (10−100 ps) than those obtained from typical THz transmitters. These tunable THz pulses are obtained by utilizing a Michelson interferometer to interfere chirped optical pulses. More recently, optical pulse shaping techniques have replaced chirped pulse interference.[227−229] This has led to greater control over the pulse duration and underlying bandwidth.

### 3.2. Pump/Probe Studies

One of the most powerful aspects of THz spectroscopy is that it provides subpicosecond pulses in the far-infrared region of the spectrum. There really is no other way to achieve this. Not surprisingly, this capability has been exploited in several ways. One is to monitor a single point on the THz waveform (or the integrated power using a bolometer), and to vary the pump−probe delay time to map out the average response of the material. A second is to map out the entire THz waveform at one or several fixed delay times after photoexcitation. Finally, the most comprehensive type of study is to create a 2D grid that maps out the THz waveform at 20−30 closely spaced pump delay times. We refer to the latter as time-resolved THz spectroscopy.

#### 3.2.1. Average Response Studies

By monitoring one point of the THz waveform, or using a bolometer to measure the THz power, it is possible to characterize the average far-IR response to an optical perturbation. It is possible to measure the overall change in transmission as well as the time scale for the system to return to its equilibrium state. Two studies of liquid solvation dynamics were reported in 1997.[230,231] Molecules with a large change in dipole moment upon photoexcitation will influence the low-frequency collective motions of nearby solvent molecules. Both found that the samples initially absorb more strongly for about 1−1.5 ps, followed by a bleach lasting roughly 3 ps. These results were interpreted as arising from a librational response of nearby solvent molecules followed by diffusive reorientation (if the excited-state lifetime of the dye molecule is sufficiently long).

A wide variety of solid samples have been investigated: bulk GaAs and InP;[48,232,233] low-temperature grown $In_{0.53}Ga_{0.47}As/In_{0.52}Al_{0.48}As$ multiple quantum wells[234] and bulklike $In_{0.53}Ga_{0.47}As$;[143] proton-bombarded InP;[235] radiation-damaged silicon-on-sapphire,[236] amorphous silicon,[237] and microcrystalline silicon;[238] self-assembled InAs/GaAs quantum dots;[239] low-temperature-grown GaAs;[142,240] functionalized pentacene molecular crystals.[241]

Dykaar and co-workers characterized the onset of photoconductivity in GaAs when photoexciting with 630 nm light and generating a carrier density of $6 \times 10^{18}$ cm$^{-3}$. They also noted that the free carriers began absorbing the THz radiation in less than 1 ps after photoexcitation.[232] By varying the excitation wavelength, they were able to probe intervalley scattering rates from the low-mobility L and X valleys back into the high-mobility Γ valley.[48,233]

The effects of Be doping in low-temperature-grown $In_{0.53}Ga_{0.47}As/In_{0.52}Al_{0.48}As$ multiple quantum wells were studied by Chen et al.[234] They compared an undoped sample with two doped ones of $5 \times 10^{17}$ and $2 \times 10^{18}$ cm$^{-3}$. They attributed the transient absorption to an increase in conductivity upon photoexcitation and noted that the transient decayed more rapidly for samples with higher doping levels. The undoped sample showed a single-exponential decay with a 16 ps time constant, the sample doped at $5 \times 10^{17}$ cm$^{-3}$ displayed a double-exponential decay with 16 and 2 ps time constants, and the sample doped at $2 \times 10^{18}$ cm$^{-3}$ had a single-exponential decay with a 1.3 ps time constant. Ralph et al.[143] showed that intervalley scattering in bulklike $In_{0.53}Ga_{0.47}As$ is well described by a three-state model[242] that consists of one state to represent the combined L and X valleys, which is coupled to a second state that is high up in the Γ valley, which in turn is coupled to a third state at the bottom of the Γ valley. Once the carriers reach the third state, they cannot scatter out of it.

Relaxation dynamics in epitaxially grown InAs/GaAs quantum dots were probed with a combination

of ultrafast scanning tunneling microscopy (STM), optical pump/probe measurements, and THz spectroscopy by Taylor et al.[239] The THz transmission measurements at pump fluences ranging from 0.1 to 10 $\mu$J cm$^{-2}$ were consistent with the ultrafast STM results.

Roskos and co-workers investigated the free carrier dynamics in LT-GaAs at moderately high excitation densities ($1.5 \times 10^{16}$ to $9 \times 10^{17}$ cm$^{-3}$).[240] Unfortunately, they only present their data in the form of transmission spectra rather than absorbance. This leads to a "nonexponential" decay that is artificial. It should be noted that determination of the time-dependent mobility is not adversely affected by treating the data this way, but it makes it more difficult to visually interpret the raw data. Prahbu et al. characterized carrier trapping rates in an LT-GaAs grown and annealed under a variety of conditions.[142] They found that the capture time increases as the anneal temperature increases, and that the capture time decreases as the amount of excess As used during the growth phase increases.

Carrier dynamics in radiation-damaged silicon-on-sapphire,[236] amorphous silicon,[237] and microcrystalline silicon[238] have been studied. Jepsen et al. find mobilities in microcrystalline silicon to be in the range of 100−1000 cm$^2$ V$^{-1}$ s$^{-1}$, and Hegmann and co-workers find the mobilities in radiation-damaged and amorphous silicon to vary from 4 to 350 cm$^2$ V$^{-1}$ s$^{-1}$ depending on the sample preparation. The heavily radiation-damaged sample has the lowest mobility, and the amorphous sample has the highest. They also find that the carrier trapping time, or relaxation time, depends on each sample: The heavily radiation-damaged sample has the shortest relaxation time, and the amorphous sample has the longest. Interestingly, the mobilities and recombination times are found to be independent of sample temperature and excitation fluence. In a similar fashion, the recombination times in proton-bombarded InP depend inversely on implantation dose.[235] However, unlike Hegmann et al.,[237] they find a dependence on excitation fluence, in which higher fluences lead to longer recombination times.

Hegmann et al. recently characterized the transient conductivity in functionalized pentacene molecular crystals.[241] By making measurements over a range of temperatures from 10 to 300 K, they showed that the carriers are a primary product of photoexcitation, and that they undergo dispersive transport at times greater than 4 ps.

### 3.2.2. Fixed Pump-Delay Studies

It is possible to obtain additional information if the entire THz waveform is collected prior to and after perturbation of the sample in some manner, such as optical excitation. This method has been used primarily to study semiconductors and superconductors, where the frequency-dependent complex-valued conductivity is obtained.

In 1992, Dykaar and co-workers probed the mobility of photoexcited electrons in GaAs 7 ps after photoexcitation.[48,233] They used bolometric detection, and therefore only measured the frequency-dependent power absorption coefficient (and not the refractive index). By fitting a parametrized Drude model to the transmission data, they extracted mobilities ranging from 1300 to 480 cm$^2$ V$^{-1}$ s$^{-1}$ when the photoexcited carrier density ranged from $0.4 \times 10^{18}$ to $5.3 \times 10^{18}$ cm$^{-3}$. Using a similar experimental setup with bolometric detection, Ralph et al. found that the Drude conductivity in bulklike $In_{0.53}Ga_{0.47}As$ varied from 5000 to 6000 cm$^2$ V$^{-1}$ s$^{-1}$ when the carrier density varied from $2.5 \times 10^{15}$ to $3.4 \times 10^{15}$ cm$^{-3}$.[143] However, they studied the dependence of decreased carrier density by waiting an additional amount of time after photoexcitation rather than by changing the fluence of the excitation beam.

Dykaar and co-workers also reported photoexcited Cooper pair breaking in superconducting Pb samples.[48,243] The far-IR transmission at the energy of the superconducting gap ($\nu_g \approx 22.5$ cm$^{-1}$) decreases on a subpicosecond time scale when the sample is rapidly laser heated above the superconducting/normal transition temperature.

Groeneveld and Grischkowsky reported population relaxation dynamics of carriers and excitons in $Al_{0.33}Ga_{0.67}As$/GaAs multiple QWs.[244] Upon photoexcitation, they monitored the decreasing broad-band, low-frequency free carrier absorption with a concomitant increase in the 1s−2p transition of heavy-hole excitons. They concluded that the 1s exciton level was populated on a time scale of a few tens of picoseconds. Bulk GaAs was studied by Flanders et al.[245] and Schall et al.[246] Flanders found that the frequency-dependent THz absorbance decreased as a function of time after photoexcitation at time delays ranging from 5 to 50 ps. The shape of the spectrum did not change, except for a scan collected at zero delay time.

Schall et al. carried out a careful study at a single point in time after photoexcitation, paying particular attention to explaining the apparent superluminal propagation of the THz pulse through the photoexcited medium.[246] That is, the peak of the THz pulse arrives roughly 50−100 fs earlier when traveling through the photoexcited sample relative to traveling through the nonphotoexcited sample. The thickness of the photoexcited layer is about 0.7 $\mu$m, and it takes light about 8.2 fs to travel this distance through a material with a refractive index of 3.5. This apparent superluminal propagation is completely understood when taking into account the complex-valued transmission and reflection coefficients. They fit the Drude model to their data and found the damping rate to be 20 THz, which corresponds to a mobility of 1300 cm$^2$ V$^{-1}$ s$^{-1}$.

The conductivity of photogenerated electrons in liquid *n*-hexane was reported by Heinz and co-workers.[247] They measured a mobility of 470 cm$^2$ V$^{-1}$ s$^{-1}$, which is far higher than the value of 0.074 cm$^2$ V$^{-1}$ s$^{-1}$ obtained with radiolysis measurements. This large difference is due to the fact that the THz measurement is sensitive to quasifree electrons, prior to trapping, whereas the radiolysis measurements are overwhelmed by the much greater fraction of bound electrons, which have much lower mobility.

Jamison et al. characterized a He discharge plasma.[248] The plasma was generated with a 50 ns rise

time pulse. They determined the time-dependent electron density and collision frequency as the plasma forms.

### *3.2.3. Time-Resolved THz Spectroscopy*

While average response and fixed pump-delay studies are quite useful, the maximum amount of information is obtained from a 2D study by taking a series of fixed pump-delay scans at a variety of times after sample photoexcition. This method is often referred to as optical pump/THz probe spectroscopy or time-resolved THz spectroscopy (TRTS).

The first such study was actually carried out in 1987 by Nuss and co-workers,[249] but it did not employ freely propagating radiation, and is therefore beyond the scope of this review. However, it deserves mention simply because it was so far ahead of its time: the next systematic two-dimensional THz study did not appear until 9 years later.[250] Nuss et al. generated THz radiation within a $LiTaO_3$ crystal which had a GaAs sample optically contacted to it, as shown in Figure 12. The THz pulse was detected after

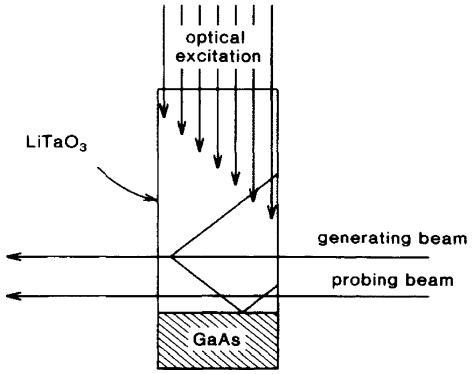


**Figure 12.** Configuration used in the original experiment to monitor the transient photoconductivity in GaAs. Reprinted with permission from ref 249. Copyright 1987 American Institute of Physics.

reflecting off the interface, and provided information about the photoinduced conductivity of the sample. They found that the mobility decreased from 4200 to 2900 $cm^2\ V^{-1}\ s^{-1}$ as the carrier density increased from $5 \times 10^{17}$ to $1.2 \times 10^{19}\ cm^{-3}$.

An optical pump/THz probe study of silicon was conducted in 1996.[250] Zielbauer et al. modeled their data with an assumed form for the input THz pulse, and found better agreement when using a time-dependent scattering rate rather than a fixed value.

In 2000 Beard et al. reported a comprehensive study of the onset of photoconductivity in single-crystalline GaAs (without any assumptions).[96] Because this system has been so well studied over the last four decades, it presented a perfect opportunity to benchmark the performance of TRTS. Effects due to surface recombination, interfacial effects at the photoexcited interface (leading to apparent superluminal propagation), proper matching of near-IR and THz spot sizes, and timing effects in regard to the sample's far-IR optical properties changing on a time scale comparable to that of the probe pulse were all addressed. It was shown that TRTS is a noncontact electrical probe with subpicosecond temporal resolution.

Leitenstorfer and co-workers carried out experiments on photoexcited bulk GaAs with much higher temporal resolution.[251−254] They employed a 10 fs duration optical pulse to generate and detect the THz pulse, which had a bandwidth of about 50 THz. They found that a plasma of correlated screened quasiparticles, which builds up from the bare charges that are formed upon absorption of the excitation pulse, occurs on a 120 fs time scale.

Kaindl et al. studied the destruction and formation of excitons in GaAs multiple QWs at a variety of temperatures.[255] Quantum well samples were used to confine the electrons and holes, rather than to investigate quantum effects. They spectrally narrowed the pump laser and used 1.540 eV photon energy to generate 1s excitons. At low temperature (6 K) the excitons recombine on a 100 ps time scale, but at higher temperature (60 K) there is significant ionization of the excitons, resulting in a conductive sample after ~100 ps. Upon increasing the photon energy to 1.561 eV and exciting into the conduction band at 6 K, the evolution from conductor to insulator was observed on a 1000 ps time scale. Interestingly, the sample became insulating because the electrons and holes formed a pure population of excitons, rather than electron−hole recombination of the initial plasma.[255]

Beard et al. extended their earlier bulk GaAs work to include characterization of carrier dynamics in LT-GaAs.[34] The carriers are trapped in the deep traps on a picosecond time scale. However, it is possible to determine their mobility during this brief period prior to being trapped since TRTS is a noncontact electrical probe with subpicosecond temporal resolution. When the carriers are photoexcited with 400 nm light, they have sufficient energy to scatter into the low-mobility L and X valleys. Thus, the conductivity will change as they simultaneously scatter back into the Γ valley ($\tau_\Gamma$ in Figure 13) and are trapped in the deep traps

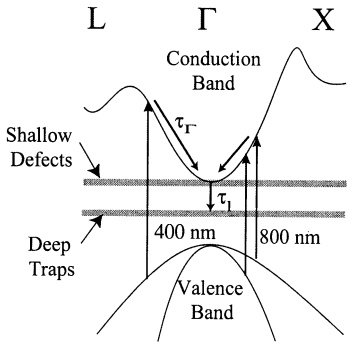


**Figure 13.** Band structure of GaAs and LT-GaAs. It is assumed that they are identical, except that LT-GaAs has shallow defects due to interstitials and lattice dislocations, as well as deep traps from the As clusters. Reprinted with permission from ref 34. Copyright 2001 American Institute of Physics.

($\tau_l$ in Figure 13).[34] The mobility increases from 350 $cm^2\ V^{-1}\ s^{-1}$ immediately after photoexcitation to 1200 $cm^2\ V^{-1}\ s^{-1}$ at 3 ps, when essentially all of the carriers have been trapped. When the carriers are excited with 800 nm light, they must remain in the

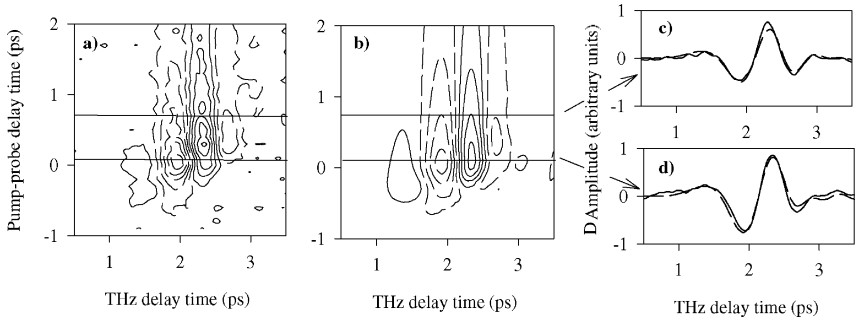


**Figure 14.** Contour plot of the 2D TRTS difference signal (THz pulse propagated through the sample with the laser on minus that with the laser off) for TBNC/chloroform. Solid contours correspond to positive values, and dashed contours are used for negative ones. Comparison of measured (a) and calculated (b) values. (c) and (d) display two representative cuts through the surfaces as indicated by the horizontal lines in (a) and (b). In (c) and (d), the measured data are shown with solid lines, and the results of the numerical propagation are shown with the dashed lines. Reprinted with permission from ref 261. Copyright 2002 American Chemical Society.

Γ valley. In this case the mobility is 3000 $cm^2\ V^{-1}\ s^{-1}$, independent of delay time, although the carriers are still trapped within 3 ps.

At this same time, Averitt et al. carried out similar studies on $YBa_2Cu_3O_{7-\delta}$ superconductors.[256,257] They fit the two-fluid model to the measured frequency- and temperature-dependent complex conductivity data, $\sigma(\omega,T)$:[258]

$$\sigma(\omega,T) = \frac{ne^2}{m^*}\left\{\frac{f_n(T)}{\tau(\omega,T)^{-1} - i\omega} + f_s(T)\left[\frac{i}{\omega} + \pi\delta(\omega)\right]\right\} \quad (1)$$

where $n$ is the total carrier concentration, $m^*$ is the effective mass, $f_n$ and $f_s$ are the normal and superconducting fractions, respectively, and $\delta$ was 0 or 0.5 for their samples. This model allows for contribution to the overall conductivity from normal quasiparticles, and from a superfluid population. Upon photoexcitation of the YBCO sample initially in its superconducting state, the superconducting pairs are broken, resulting in an increase in $f_n$ and a concomitant decrease in $f_s$. The superconducting pair recovery time, $\tau_\sigma$, is on a picosecond time scale, but there is also a much slower component on a nanosecond time scale that is attributed to generation of phonons which must first be thermally transported to the substrate before the sample can fully cool. They find that, for the optimally doped sample ($\delta = 0.0$), $\tau_\sigma$ increases from ~1.5 ps at 4 K to ~3.5 ps near $T_c$ (85 K). Unlike THz emission studies of superconductors, these experiments provide the full frequency-dependent complex conductivity as a function of time after photoexcitation.

Averitt et al. also carried out TRTS studies of colossal magnetoresistance manganite thin films of $La_{0.7}Ca_{0.3}MnO_3$ and $La_{0.7}Sr_{0.3}MnO_3$.[259] They varied the temperature from 15 K to $T_c$ (250 K for $La_{0.7}Ca_{0.3}MnO_3$ and 360 K for $La_{0.7}Sr_{0.3}MnO_3$). Upon photoexcitation, they found a conductivity decrease on a 2 ps time scale, and attributed it to modification of the phonon temperature. There was also a slower component, which is related to spin−lattice relaxation. Its lifetime increases in going from low temperature to $T_c$. It is about 5−10 ps at low temperature, and about 60−80 ps at $T_c$.

Beard et al. characterized the solvent response to photoexcitation of a nearby dye molecule.[260,261] They photoexcited TBNC (2,11,20,29-tetra-*tert*-butyl-2,3-naphthalocyanine) dissolved in chloroform and toluene. The 2D data set is shown in Figure 14. The solvent response was modeled as a (multipole) Lorentzian oscillator representing the low-frequency collective mode(s). An instantaneous electronic contribution was required in addition to the solvent modes. The recovery time, $\tau_r$, of toluene is 0.5 ps, and the overdamped solvent mode becomes underdamped during this period. For chloroform, $\tau_r$ is 1.4 ps, and the underdamped librational mode centered near 42 $cm^{-1}$ becomes highly overdamped for the solvent molecules near the TBNC dye (see Figure 15).

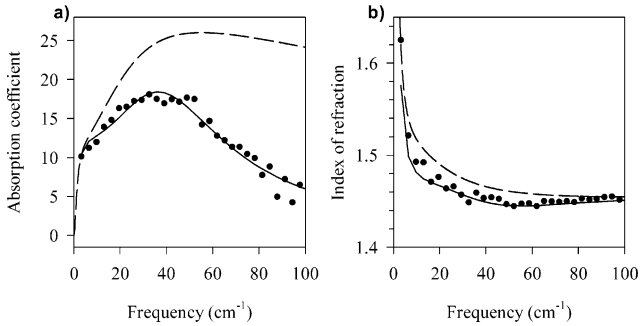


**Figure 15.** Frequency-dependent absorption coefficient and refractive index of $CHCl_3$ under steady-state conditions (filled circles and best fit solid line), and after photoexcitation of a nearby dye molecule (dashed line). It is seen that the mode centered at 42 $cm^{-1}$ becomes overdamped during the reorientation process. Reprinted with permission from ref 261. Copyright 2002 American Chemical Society.

Transient photoconductivity in CdSe nanoparticles (NPs) and nanocrystalline $TiO_2$ has recently been investigated.[262,263] Beard et al. studied the dependence of transient photoconductivity in CdSe NPs.[262] They found that the biexponential recovery time depended linearly on NP diameter, indicating ballistic transport to the surface, rather than diffusive transport. For NPs larger than the Bohr radius (4.9 nm for CdSe) they found that the mobility scaled as $1/l_{bulk} + 1/r_{NP}$, where $l_{bulk}$ is the bulk mean free path and $r_{NP}$ is the NP radius, and for NPs smaller than $r_{NP}$, it scaled as $r^4$. For NPs smaller than $r_{NP}$, it is

not appropriate to describe their response in terms of mobility, since the carriers are not mobile. Instead, the THz transient response is due to the NPs' polarizability, but since the model did not explicitly include polarizability, it was attributed to mobility. Turner et al. probed the transient photoconductivity in colloidal, nanocrystalline $TiO_2$.[263] They found that the carriers strongly backscatter, leading to a negative imaginary conductivity.[264] They also found that the photoinjected electrons thermalize with a time constant of roughly 400 fs. Both of these studies utilize the fact that TRTS is a noncontact electrical probe with subpicosecond temporal resolution, and this level of detail could not be obtained in any other way.

#### 3.2.4. THz Pump/Optical Probe Studies

Cook and Hochstrasser carried out a different sort of time-resolved THz study. It is the time-resolved analogue of electric-field-induced second harmonic generation, and is referred to as THz field-induced second harmonic generation.[265] It is known that an isotropic medium does not generate second harmonic frequencies. However, if a large electric field is applied to the sample and the molecules either are polar or have a polarizability anisotropy, then the second harmonic frequency can be generated. They characterized dynamics in neat acetonitrile and water by varying the arrival time of the optical pulse relative to the terahertz pulse.

### 3.3. Coherent Control

Over the last 10 years, Bucksbaum and co-workers have carried out an intensive investigation of Rydberg atom dynamics via interaction with THz half-cycle pulses (HCPs).[266−274] The earliest papers used the HCPs to ionize Rydberg atoms.[268−270] Here they showed that an HCP could ionize the Rydberg atom when the electron was traveling anywhere throughout its Keplerian orbit, whereas it is well-known that optical pulses only ionize Rydberg atoms when the electron is close to the nucleus. This is because the integral of the time-varying electromagnetic amplitude of an optical pulse is zero, and the electron can only acquire the requisite momentum for ionization by scattering off the nucleus. On the other hand, when an HCP is used, it can impart momentum to the electron throughout its orbit. It is true that the integral of the HCP is zero as well, but there is a large asymmetry: There is a large field for several hundred femtoseconds, followed by a very weak field of opposite polarity for tens to hundreds of picoseconds, so in effect, the electrons are interacting with a unipolar pulse. This same methodology was used with shorter excitation pulses, on the order of 1 ps, to map out the Rydberg wave packet motion of atomic Cs. This type of experiment has also been studied theoretically.[275] More recently, Bucksbaum et al. have explored phase retrieval,[266,272] quantum-state information retrieval,[267] and control of Rydberg atoms to perform Grover's search algorithm.[273] When implementing Grover's search algorithm, they found that an optimally shaped THz pulse performed better than an unshaped HCP.

In a related direction, van Driel, Sipe, and co-workers have experimentally and theoretically probed coherent photocurrent generation in bulk semiconductors. In this work, the THz pulse generated is a diagnostic rather than a driving field. Initially, they measured the photocurrent and/or photovoltage as a function of phase delay between two optical pulses where one (the fundamental) is below the band gap and the other (its second harmonic) is above the band gap.[276,277] Later work demonstrated that THz emission accompanied this transient photocurrent, and it could also be coherently controlled as a function of the phase of the two excitation beams.[278] They clearly demonstrated that several different processes, such as rectification and shift current, contribute to THz generation.[279]

## 4. Theory

The emphasis of this review is experimental work. However, there have been several theoretical/computational efforts directed at understanding the phenomena described here, so that work will be reviewed. Naturally, most experimental papers include theory at the level of extracting dynamical information through an appropriate model, but this section concentrates on papers whose primary focus is theoretical in nature. These papers can be loosely grouped into three categories: (1) understanding generation and detection, typically in regard to photoconductive antennas,[27,28,30,54,115,122,280−284] (2) issues related to THz pulse propagation,[260,285−289] and (3) understanding phenomena observed in specific types of THz experiments.[64,73,74,290−292]

### 4.1. Generation and Detection

One of the first theoretical treatments of THz generation and detection focused on the influence of the hyperhemispherical lens attached to the back of the generation wafer on the emitted radiation pattern.[280] Jepsen et al. found that experimentally obtained spatial patterns were very well fit by calculations based on Huygen's principle of superposition of secondary wavelets. More recently, Chung et al. have employed finite-difference time-domain (FDTD) calculations along with diffraction theory to characterize THz generation in a Hertzian dipole antenna coupled with a hyperhemispherical lens.[28]

Joshi et al. used Monte Carlo simulations to understand energy loss properties of carriers in photoexcited THz transmitters.[281] Monte Carlo calculations were also used by Abe et al. to investigate transient carrier velocities in photoexcited GaAs.[283] In 1994 Khurgin described optical rectification and THz emission in zinc blende semiconductors, and found that intraband relaxation processes play an important role.[282] Piao et al. calculated the generation of THz radiation from a biased photoconductive antenna, and attributed most of the signal to the rapid change in carrier density due to photoexcitation with an ultrafast optical pulse, as opposed to carrier acceleration.[284] They also found that the THz waveform is distorted when detected with a photoconductive antenna. Similarly, Chen and co-workers employed FDTD methodology to model a photoconductive antenna, and found reasonable agreement with ex-

perimental measurements.[27] THz emission from photoconductive antennas has also been modeled analytically by Duvillaret et al.[30] They evaluated the influence of parameters such as free carrier lifetime, carrier collision time, and optical pulse duration on the THz bandwidth, power, and signal-to-noise ratio. Malevich performed Monte Carlo simulations of THz generation from the semiconductor surface depletion field, and included acoustic, optical, and intervalley phonon scattering.[54] He found that the photocarrier-induced screening of the depletion field depends on the doping level, and the photon energy and intensity of the excitation pulse.

Park et al. compared the measurement of THz waveforms with photoconductive antennas and electrooptic sampling.[122] They related the two techniques, and investigated the role of photoconductive antenna response and carrier lifetime. Sun et al. analyzed measurement of a THz pulse with a chirped probe beam, as used in single-shot measurements.[115] They discussed the dependence of the temporal resolution on the chirp rate and spectrum of the probe beam, as well as the resolution of the spectrometer.

### 4.2. Propagation

Studies of the propagation of THz pulses began in 1997 with a paper by You and Bucksbaum treating free space propagation as well as propagation through apertures and focusing optics.[285] Kuzel et al. considered similar issues, except concentrated on large-aperture emitters, and found impressive agreement with experimental results.[286]

Beard and Schmuttenmaer asserted (incorrectly) that the only way to simulate a TRTS experiment wherein the optical properties of the medium were changing on the time scale of the THz pulse (for which the slowly varying envelope and rotating wave approximations are not valid) was through a numerical FDTD treatment.[260] They described the method and applied it to the solvent response to photoexcitation of a solvated dye molecule. Nemec et al. proposed an analytical frequency-domain methodology for achieving the same result, but did not apply it to actual data, nor did they clearly describe how other workers could analyze actual data using their method.[288] Very recently, a simple analytical model for THz propagation in experimental situations has been described.[289] In addition to addressing issues of polarization, focusing optics, and angle-dependent reflection and transmission, they have made comparisons to experimental results. Nekkanti et al. performed a three-dimensional FDTD simulation of THz pulse shaping by conductive apertures, and also implemented an analytical near-field to far-field transform to dramatically reduce the computational time required.[287]

### 4.3. Specific Experiments

Excitonic Bloch oscillations driven by a THz field in a semiconductor superlattice have been treated by Lachaine et al.[290] They found that interaction of electron−hole pairs is essential for stimulated THz emission. Feise et al. explored harmonic generation of a THz driving field in a semiconductor superlattice and predict a sharp high-frequency cutoff.[293]

The magnetic field enhancement of THz generation discussed in section 2.3 has been considered by several authors. Shan et al. found that the Drude−Lorentz model coupled with properties of the semiconductor−air interface could explain the experimentally observed enhancement.[73] Similarly, a Monte Carlo simulation of the carrier dynamics along with considerations for the surface interface accounted for the magnetic field enhancement.[74]

Okumura and Tanimura proposed a 2D THz study of liquid water.[291] They modeled the spectrum of water as two Brownian oscillators, and showed how the measured third-order nonlinear response would depend sensitively on whether the low-frequency or high-frequency mode was anharmonic. Kindt et al. presented an overview of the manifestation of changes in the low-frequency solvent modes due to photoexcitation of a nearby dye molecule.[292] They paid particular attention to the evolution of the THz spectrum as a function of time after photoexcitation.

## 5. Conclusions

The emergence of femtochemistry (and femtoscience in general) over the last two decades has provided unprecedented new insight into the nature of molecular vibrations, electron transfer in biological and nonbiological systems, carrier dynamics in semiconductors, gas-phase processes such as dissociation, isomerization, and photoelectron spectroscopy, protein dynamics, and even control over molecular processes. Time-resolved THz spectroscopy has opened a window into the far-IR region of the spectrum for this type of work. It is clear from merely scanning through the references at the end of this review that utilizing THz spectroscopy to understand dynamics has been dominated by solid-state physicists. However, the sheer number of papers indicates that time-resolved THz spectroscopy provides otherwise unobtainable information on dynamics in the FIR, which indicates a general usefulness. While experimental TRTS is not trivial, and there are a variety of potential pitfalls that must be avoided, it is no more complicated than the type of experiments performed routinely by femtochemists worldwide. It is just a matter of time before chemical and biological systems are studied with the same vigor already seen in solid-state physics.

In the chemistry community, there will be a great deal of activity within the next decade, generally in the fields of nonlinear optics, materials science, nanoscience, molecular electronics, and biophysical applications.

Nonlinear experiments involving only THz pulses will emerge, that is, THz pump/THz probe spectroscopy and 2D THz spectroscopy. For example, this will allow intermolecular couplings in liquids to be monitored in a fashion similar to that of intramolecular or electronic couplings measured in 2D IR[294,295] and optical spectroscopies,[296] respectively, which are analogous in many respects to 2D NMR experiments. The ability to easily characterize and control the phase of the THz pulses will be a distinct advantage. In

addition to nonlinear interactions in neat liquids, large molecules of biophysical interest with low-frequency modes in solution will be probed. This could even lead to detailed investigation of the nature of the coupling between modes involving secondary structure in proteins such as α-helices and β-sheets.[297] There exist low-frequency intermolecular modes (librons) in amino acid crystals that fall in the far-IR.[298] Given that these are large-amplitude motions, they are expected to be anharmonic and coupled to each other. Two-dimensional THz experiments will reveal the underlying nature of the anharmonicity and coupling among intermolecular modes.

In the fields of materials science, nanoscience, and molecular electronics, TRTS will prove especially valuable in the context of being a noncontact electrical probe with subpicosecond time resolution. This will aid in characterizing the intrinsic electrical properties of these materials in the context of their potential advantages in optoelectronic devices, among other things. Carrier dynamics in isolated NPs, isolated core−shell NPs, quantum rods and quantum disks (where anisotropic effects are expected), disordered NP arrays,[299] and NP periodic arrays (or artificial solids) will all be of importance. For bulk materials, time-resolved phonon dynamics will also be accessible through either a THz or optical excitation pulse, followed by a THz probe pulse.

THz emission spectroscopy will provide valuable insight into the nature of charge motion in the field of molecular electronics. There can be ambiguity as to whether molecular properties or the nearby environment is probed with currently used methods involving STM or conventional conductivity measurements.[300] THz emission spectroscopy of oriented molecular monolayers, bilayers, or more sophisticated device geometries will provide a complimentary method of characterization. THz emission spectroscopy will also provide insight into intra- and intermolecular charge transfer in molecular crystals upon photoexcitation.[102] It will also be used as an alternative probe of ultrafast demagnetization by monitoring the THz pulse emitted due to an ultrafast laser-induced change in the magnetization of a sample.[301]

This review has primarily focused on a wide variety of experimental results and experimental considerations, although important theoretical contributions have been noted. Time-resolved THz spectroscopy has successfully lived through its infancy, and now stands as a robust method for characterizing dynamics in the far-IR. Initial studies have revealed the time scales of fundamental processes primarily in solid-state systems, such as bulk semiconductors, semiconductor heterostructures and quantum wells, and superconductors. However, several studies of molecular processes and material properties described in this review demonstrate its broad versatility.

## 6. Supporting Information Available

The entire list of references with their titles is available free of charge via the Internet at http://pubs.acs.org.

## 7. References


(1) Nuss, M. C.; Orenstein, J. In *Millimeter and Submillimeter Wave Spectroscopy of Solids*; Gruner, G., Ed.; Springer-Verlag: Berlin, 1998; Vol. 74.
(2) Mittleman, D. *Sensing with Terahertz Radiation*; Springer-Verlag: Berlin, 2003.
(3) Siegel, P. H. *IEEE Trans. Microwave Theory Tech.* **2002**, *50*, 910.
(4) Beard, M. C.; Turner, G. M.; Schmuttenmaer, C. A. *J. Phys. Chem. B* **2002**, *106*, 7146.
(5) Han, P. Y.; Zhang, X. C. *Meas. Sci. Technol.* **2001**, *12*, 1747.
(6) Ferguson, B.; Zhang, X. C. *Nat. Mater.* **2002**, *1*, 26.
(7) Averitt, R. D.; Taylor, A. J. *J. Phys.: Condens. Matter* **2002**, *14*, R1357.
(8) Shan, J.; Nahata, A.; Heinz, T. F. *J. Nonlinear Opt. Phys. Mater.* **2002**, *11*, 31.
(9) Davies, A. G.; Linfield, E. H.; Johnston, M. B. *Phys. Med. Biol.* **2002**, *47*, 3679.
(10) Kawase, K.; Shikata, J.; Ito, H. *J. Phys. D: Appl. Phys.* **2002**, *35*, R1.
(11) Kimmitt, M. F. *J. Biol. Phys.* **2003**, *29*, 77.
(12) *Proceedings of the First International Conference on Biomedical Imaging and Sensing Applications of THz Technology* (Special Issue); *Phys. Med. Biol.* **2002**, *47*.
(13) *J. Biol. Phys.* **2003**, *29*.
(14) Smith, P. R.; Auston, D. H.; Nuss, M. C. *IEEE J. Quantum Electron.* **1988**, *24*, 255.
(15) Fattinger, C.; Grischkowsky, D. *Appl. Phys. Lett.* **1989**, *54*, 490.
(16) van Exter, M.; Fattinger, C.; Grischkowsky, D. *Appl. Phys. Lett.* **1989**, *55*, 337.
(17) van Exter, M.; Grischkowsky, D. R. *IEEE Trans. Microwave Theory Tech.* **1990**, *38*, 1684.
(18) Ralph, S. E.; Grischkowsky, D. *Appl. Phys. Lett.* **1991**, *59*, 1972.
(19) Katzenellenbogen, N.; Grischkowsky, D. *Appl. Phys. Lett.* **1991**, *58*, 222.
(20) Warren, A. C.; Katzenellenbogen, N.; Grischkowsky, D.; Woodall, J. M.; Melloch, M. R.; Otsuka, N. *Appl. Phys. Lett.* **1991**, *58*, 1512.
(21) Ludwig, C.; Kuhl, J. *Appl. Phys. Lett.* **1996**, *69*, 1194.
(22) Heiliger, H. M.; Vosseburger, M.; Roskos, H. G.; Kurz, H.; Hey, R.; Ploog, K. *Appl. Phys. Lett.* **1996**, *69*, 2903.
(23) Tani, M.; Matsuura, S.; Sakai, K.; Nakashima, S. *Appl. Opt.* **1997**, *36*, 7853.
(24) Lin, P. I.; Chen, S. F.; Wu, K. H.; Juang, J. Y.; Uhn, T. M.; Gou, Y. S. *Jpn. J. Appl. Phys., Part 2* **2002**, *41*, L1158.
(25) Liu, T. A.; Tani, M.; Pan, C. L. *J. Appl. Phys.* **2003**, *93*, 2996.
(26) Pedersen, J. E.; Keiding, S. R.; Sorensen, C. B.; Lindelof, P. E.; Ruhle, W. W.; Zhou, X. Q. *J. Appl. Phys.* **1993**, *74*, 7022.
(27) Zhang, J. Z.; Chen, Z. Z.; Chen, X. M. *Int. J. RF Microwave Comput.-Aided Eng.* **2000**, *10*, 213.
(28) Chung, Y. S.; Cheon, C.; Son, J. H.; Hahn, S. Y. *IEEE Trans. Magn.* **2000**, *36*, 951.
(29) Jepsen, P. U.; Jacobsen, R. H.; Keiding, S. R. *J. Opt. Soc. Am. B* **1996**, *13*, 2424.
(30) Duvillaret, L.; Garet, F.; Roux, J. F.; Coutaz, J. L. *IEEE J. Sel. Top. Quantum Electron.* **2001**, *7*, 615.
(31) Kindt, J. T.; Schmuttenmaer, C. A. *J. Phys. Chem.* **1996**, *100*, 10373.
(32) Melloch, M. R.; Woodall, J. M.; Harmon, E. S.; Otsuka, N.; Pollak, F. H.; Nolte, D. D.; Feenstra, R. M.; Lutz, M. A. *Annu. Rev. Mater. Sci.* **1995**, *25*, 547.
(33) Wang, H. H.; Whitaker, J. F.; Chin, A.; Mazurowski, J.; Ballingall, J. M. *J. Electron. Mater.* **1993**, *22*, 1461.
(34) Beard, M. C.; Turner, G. M.; Schmuttenmaer, C. A. *J. Appl. Phys.* **2001**, *90*, 5915.
(35) Tonouchi, M.; Tani, M.; Wang, Z.; Sakai, K.; Hangyo, M.; Wada, N.; Murakami, Y. *IEEE Trans. Appl. Supercond.* **1997**, *7*, 2913.
(36) Tani, M.; Tonouchi, M.; Hangyo, M.; Wang, Z.; Onodera, N.; Sakai, K. *Jpn. J. Appl. Phys., Part 1* **1997**, *36*, 1984.
(37) Tanichi, N.; Wada, N.; Nagashima, T.; Tonouchi, M.; Hangyo, M.; Tani, M.; Sakai, K. *Physica C* **1997**, *293*, 229.
(38) Shikii, S.; Tanichi, N.; Nagashima, T.; Tonouchi, M.; Hangyo, M.; Tani, M.; Sakai, K. *IEICE Trans. Electron.* **1997**, *E80C*, 1297.
(39) Pedersen, J. E.; Balslev, I.; Hvam, J. M.; Keiding, S. R. *Appl. Phys. Lett.* **1992**, *61*, 1372.
(40) Andrews, S. R.; Armitage, A.; Huggard, P. G.; Hussain, A. *Phys. Med. Biol.* **2002**, *47*, 3705.
(41) Xu, L.; Zhang, X. C.; Auston, D. H.; Jalali, B. *Appl. Phys. Lett.* **1991**, *59*, 3357.
(42) Zhang, X. C.; Auston, D. H. *J. Electromagn. Waves Appl.* **1992**, *6*, 85.
(43) Hu, B. B.; Weling, A. S.; Auston, D. H.; Kuznetsov, A. V.; Stanton, C. J. *Phys. Rev. B* **1994**, *49*, 2234.
(44) Leitenstorfer, A.; Hunsche, S.; Shah, J.; Nuss, M. C.; Knox, W. H. *Appl. Phys. Lett.* **1999**, *74*, 1516.
(45) Zhang, X. C.; Darrow, J. T.; Hu, B. B.; Auston, D. H.; Schmidt, M. T.; Tham, P.; Yang, E. S. *Appl. Phys. Lett.* **1990**, *56*, 2228.

(46) Jin, Y.; Ma, X. F.; Wagoner, G. A.; Alexander, M.; Zhang, X. C. *Appl. Phys. Lett.* **1994**, *65*, 682.
(47) Zhang, X. C.; Hu, B. B.; Darrow, J. T.; Auston, D. H. *Appl. Phys. Lett.* **1990**, *56*, 1011.
(48) Greene, B. I.; Saeta, P. N.; Dykaar, D. R.; Schmittrink, S.; Chuang, S. L. *IEEE J. Quantum Electron.* **1992**, *28*, 2302.
(49) Li, M.; Sun, F. G.; Wagoner, G. A.; Alexander, M.; Zhang, X. C. *Appl. Phys. Lett.* **1995**, *67*, 25.
(50) Kondo, T.; Sakamoto, M.; Tonouchi, M.; Hangyo, M. *Jpn. J. Appl. Phys., Part 2* **1999**, *38*, L1035.
(51) Han, P. Y.; Huang, X. G.; Zhang, X. C. *Appl. Phys. Lett.* **2000**, *77*, 2864.
(52) Kono, S.; Gu, P.; Tani, M.; Sakai, K. *Appl. Phys. B* **2000**, *71*, 901.
(53) Gu, P.; Tani, M.; Kono, S.; Sakai, K.; Zhang, X. C. *J. Appl. Phys.* **2002**, *91*, 5533.
(54) Malevich, V. L. *Semicond. Sci. Technol.* **2002**, *17*, 551.
(55) Nakajima, M.; Takahashi, M.; Hangyo, M. *Appl. Phys. Lett.* **2002**, *81*, 1462.
(56) Zhang, X. C.; Jin, Y.; Hewitt, T. D.; Sangsiri, T.; Kingsley, L. E.; Weiner, M. *Appl. Phys. Lett.* **1993**, *62*, 2003.
(57) Sarukura, N.; Ohtake, H.; Izumida, S.; Liu, Z. L. *J. Appl. Phys.* **1998**, *84*, 654.
(58) Izumida, S.; Ono, S.; Liu, Z. L.; Ohtake, H.; Sarukura, N. *Appl. Phys. Lett.* **1999**, *75*, 451.
(59) Ono, S.; Tsukamoto, T.; Sakai, M.; Liu, Z. L.; Ohtake, H.; Sarukura, N.; Nishizawa, S.; Nakanishi, A.; Yoshida, M. *Rev. Sci. Instrum.* **2000**, *71*, 554.
(60) McLaughlin, R.; Chen, Q.; Corchia, A.; Ciesla, C. M.; Arnone, D. D.; Zhang, X. C.; Jones, G. A. C.; Lindfield, E. H.; Pepper, M. *J. Mod. Opt.* **2000**, *47*, 1847.
(61) Ohtake, H.; Ono, S.; Sakai, M.; Liu, Z. L.; Tsukamoto, T.; Sarukura, N. *Appl. Phys. Lett.* **2000**, *76*, 1398.
(62) Ohtake, H.; Ono, S.; Sakai, M.; Liu, Z.; Sarukura, N. *J. Lumin.* **2000**, *87*−*9*, 902.
(63) Liu, Z. L.; Ohtake, H.; Izumida, S.; Ono, S.; Sarukura, N. *Opt. Quantum Electron.* **2000**, *32*, 521.
(64) Heyman, J. N.; Neocleous, P.; Hebert, D.; Crowell, P. A.; Muller, T.; Unterrainer, K. *Phys. Rev. B* **2001**, *64*, 085202.
(65) Ono, S.; Tsukamoto, T.; Kawahata, E.; Yano, T.; Ohtake, H.; Sarukura, N. *Appl. Opt.* **2001**, *40*, 1369.
(66) Migita, M.; Hangyo, M. *Appl. Phys. Lett.* **2001**, *79*, 3437.
(67) Ohtake, H.; Suzuki, Y.; Sarukura, N.; Ono, S.; Tsukamoto, T.; Nakanishi, A.; Nishizawa, S.; Stock, M. L.; Yoshida, M.; Endert, H. *Jpn. J. Appl. Phys., Part 2* **2001**, *40*, L1223.
(68) Hangyo, M.; Migita, M.; Nakayama, K. *J. Appl. Phys.* **2001**, *90*, 3409.
(69) Ohtake, H.; Murakami, H.; Yano, T.; Ono, S.; Sarukura, N.; Takahashi, H.; Suzuki, Y.; Nishijima, G.; Watanabe, K. *Appl. Phys. Lett.* **2003**, *82*, 1164.
(70) Weiss, C.; Wallenstein, R.; Beigang, R. *Appl. Phys. Lett.* **2000**, *77*, 4160.
(71) Johnston, M. B.; Corchia, A.; Dowd, A.; Linfield, E. H.; Davies, A. G.; McLaughlin, R.; Arnone, D. D.; Pepper, M. *Physica E* **2002**, *13*, 896.
(72) Takahashi, H.; Suzuki, Y.; Sakai, M.; Ono, S.; Sarukura, N.; Sugiura, T.; Hirosumi, T.; Yoshida, M. *Appl. Phys. Lett.* **2003**, *82*, 2005.
(73) Shan, J.; Weiss, C.; Wallenstein, R.; Beigang, R.; Heinz, T. F. *Opt. Lett.* **2001**, *26*, 849.
(74) Johnston, M. B.; Whittaker, D. M.; Corchia, A.; Davies, A. G.; Linfield, E. H. *J. Appl. Phys.* **2002**, *91*, 2104.
(75) Johnston, M. B.; Whittaker, D. M.; Corchia, A.; Davies, A. G.; Linfield, E. H. *Phys. Rev. B* **2002**, *65*, 165301.
(76) Andrews, S. R.; Armitage, A.; Huggard, P. G.; Shaw, C. J.; Moore, G. P.; Grey, R. *Phys. Rev. B* **2002**, *66*, 085307.
(77) Sarukura, N.; Liu, Z.; Ohtake, H.; Izumida, S.; Yamanaka, T.; Segawa, Y.; Itatani, T.; Sugaya, T.; Nakagawa, T.; Sugiyama, Y. *Jpn. J. Appl. Phys., Part 2* **1997**, *36*, L560.
(78) Sarukura, N.; Ohtake, H.; Liu, Z.; Itatani, T.; Sugaya, T.; Nakagawa, T.; Sugiyama, Y. *Jpn. J. Appl. Phys., Part 2* **1998**, *37*, L125.
(79) Liu, T. A.; Huang, K. F.; Pan, C. L.; Liu, Z. L.; Ono, S.; Ohtake, H.; Sarukura, N. *Jpn. J. Appl. Phys., Part 2* **1999**, *38*, L1333.
(80) Liu, Z. L.; Ono, S.; Ohtake, H.; Sarukura, N.; Liu, T. A.; Huang, K. F.; Pan, C. L. *Jpn. J. Appl. Phys., Part 2* **2000**, *39*, L366.
(81) Darrow, J. T.; Hu, B. B.; Zhang, X. C.; Auston, D. H. *Opt. Lett.* **1990**, *15*, 323.
(82) Darrow, J. T.; Zhang, X. C.; Auston, D. H. *Appl. Phys. Lett.* **1991**, *58*, 25.
(83) Benicewicz, P. K.; Roberts, J. P.; Taylor, A. J. *J. Opt. Soc. Am. B* **1994**, *11*, 2533.
(84) You, D.; Jones, R. R.; Bucksbaum, P. H.; Dykaar, D. R. *Opt. Lett.* **1993**, *18*, 290.
(85) Hattori, T.; Tukamoto, K.; Nakatsuka, H. *Jpn. J. Appl. Phys., Part 1* **2001**, *40*, 4907.
(86) Zhao, G.; Schouten, R. N.; van der Valk, N.; Wenckebach, W. T.; Planken, P. C. M. *Rev. Sci. Instrum.* **2002**, *73*, 1715.
(87) Auston, D. H.; Nuss, M. C. *IEEE J. Quantum Electron.* **1988**, *24*, 184.
(88) Carrig, T. J.; Rodriguez, G.; Clement, T. S.; Taylor, A. J.; Stewart, K. R. *Appl. Phys. Lett.* **1995**, *66*, 121.
(89) Chen, Q.; Zhang, X. C. *Appl. Phys. Lett.* **1999**, *74*, 3435.
(90) Hu, B. B.; Zhang, X. C.; Auston, D. H.; Smith, P. R. *Appl. Phys. Lett.* **1990**, *56*, 506.
(91) Nahata, A.; Weling, A. S.; Heinz, T. F. *Appl. Phys. Lett.* **1996**, *69*, 2321.
(92) Rice, A.; Jin, Y.; Ma, X. F.; Zhang, X. C.; Bliss, D.; Larkin, J.; Alexander, M. *Appl. Phys. Lett.* **1994**, *64*, 1324.
(93) Xu, L.; Zhang, X. C.; Auston, D. H. *Appl. Phys. Lett.* **1992**, *61*, 1784.
(94) Zhang, X. C.; Jin, Y.; Ma, X. F. *Appl. Phys. Lett.* **1992**, *61*, 2764.
(95) Han, P. Y.; Zhang, X. C. *Appl. Phys. Lett.* **1998**, *73*, 3049.
(96) Beard, M. C.; Turner, G. M.; Schmuttenmaer, C. A. *Phys. Rev. B* **2000**, *62*, 15764.
(97) Reimann, K.; Smith, R. P.; Weiner, A. M.; Elsaesser, T.; Woerner, M. *Opt. Lett.* **2003**, *28*, 471.
(98) Han, P. Y.; Cho, G. C.; Zhang, X. C. *J. Nonlinear Opt. Phys. Mater.* **1999**, *8*, 89.
(99) Huber, R.; Brodschelm, A.; Tauser, F.; Leitenstorfer, A. *Appl. Phys. Lett.* **2000**, *76*, 3191.
(100) Sinyukov, A. M.; Hayden, L. M. *Opt. Lett.* **2002**, *27*, 55.
(101) Han, P. Y.; Tani, M.; Pan, F.; Zhang, X. C. *Opt. Lett.* **2000**, *25*, 675.
(102) Carey, J. J.; Bailey, R. T.; Pugh, D.; Sherwood, J. N.; Cruickshank, F. R.; Wynne, K. *Appl. Phys. Lett.* **2002**, *81*, 4335.
(103) Jiang, Z. P.; Zhang, X. C. *IEEE Trans. Microwave Theory Tech.* **1999**, *47*, 2644.
(104) Wu, Q.; Hewitt, T. D.; Zhang, X. C. *Appl. Phys. Lett.* **1996**, *69*, 1026.
(105) Wu, Q.; Zhang, X. C. *Appl. Phys. Lett.* **1997**, *71*, 1285.
(106) Wu, Q.; Litz, M.; Zhang, X. C. *Appl. Phys. Lett.* **1996**, *68*, 2924.
(107) Wu, Q.; Zhang, X. C. *Appl. Phys. Lett.* **1996**, *68*, 1604.
(108) Bakker, H. J.; Cho, G. C.; Kurz, H.; Wu, Q.; Zhang, X. C. *J. Opt. Soc. Am. B* **1998**, *15*, 1795.
(109) Gallot, G.; Grischkowsky, D. *J. Opt. Soc. Am. B* **1999**, *16*, 1204.
(110) Planken, P. C. M.; Nienhuys, H. K.; Bakker, H. J.; Wenckebach, T. *J. Opt. Soc. Am. B* **2001**, *18*, 313.
(111) Vosseburger, M.; Brucherseifer, M.; Cho, G. C.; Roskos, H. G.; Kurz, H. *Appl. Opt.* **1998**, *37*, 3368.
(112) Jiang, Z. P.; Zhang, X. C. *Opt. Lett.* **1998**, *23*, 1114.
(113) Jiang, Z. P.; Zhang, X. C. *Appl. Phys. Lett.* **1998**, *72*, 1945.
(114) Jiang, Z. P.; Zhang, X. C. *IEEE J. Quantum Electron.* **2000**, *36*, 1214.
(115) Sun, F. G.; Jiang, Z. P.; Zhang, X. C. *Appl. Phys. Lett.* **1998**, *73*, 2233.
(116) Shan, J.; Weling, A. S.; Knoesel, E.; Bartels, L.; Bonn, M.; Nahata, A.; Reider, G. A.; Heinz, T. F. *Opt. Lett.* **2000**, *25*, 426.
(117) Kaindl, R. A.; Eickemeyer, F.; Woerner, M.; Elsaesser, T. *Appl. Phys. Lett.* **1999**, *75*, 1060.
(118) Bonvalet, A.; Joffre, M.; Martin, J. L.; Migus, A. *Appl. Phys. Lett.* **1995**, *67*, 2907.
(119) Kono, S.; Tani, M.; Sakai, K. *IEE Proc.: Optoelectron.* **2002**, *149*, 105.
(120) Kono, S.; Tani, M.; Sakai, K. *Appl. Phys. Lett.* **2001**, *79*, 898.
(121) Park, S. G.; Melloch, M. R.; Weiner, A. M. *Appl. Phys. Lett.* **1998**, *73*, 3184.
(122) Park, S. G.; Melloch, M. R.; Weiner, A. M. *IEEE J. Quantum Electron.* **1999**, *35*, 810.
(123) Kawase, K.; Sato, M.; Taniuchi, T.; Ito, H. *Appl. Phys. Lett.* **1996**, *68*, 2483.
(124) Kawase, K.; Sato, M.; Nakamura, K.; Taniuchi, T.; Ito, H. *Appl. Phys. Lett.* **1997**, *71*, 753.
(125) Kawase, K.; Shikata, J.; Sato, M.; Taniuchi, T.; Ito, H. *Electron. Commun. Jpn., Part II* **1998**, *81*, 10.
(126) Ito, H.; Kawase, K.; Shikata, J. *IEICE Trans. Electron.* **1998**, *E81C*, 264.
(127) Shikata, J.; Sato, M.; Taniuchi, T.; Ito, H. *Opt. Lett.* **1999**, *24*, 202.
(128) Shikata, J.; Kawase, K.; Karino, K.; Taniuchi, T.; Ito, H. *IEEE Trans. Microwave Theory Tech.* **2000**, *48*, 653.
(129) Sato, A.; Kawase, K.; Minamide, H.; Wada, S.; Ito, H. *Rev. Sci. Instrum.* **2001**, *72*, 3501.
(130) Lee, Y. S.; Norris, T. B. *J. Opt. Soc. Am. B* **2002**, *19*, 2791.
(131) Kawase, K.; Hatanaka, T.; Takahashi, H.; Nakamura, K.; Taniuchi, T.; Ito, H. *Opt. Lett.* **2000**, *25*, 1714.
(132) Weiss, C.; Torosyan, G.; Avetisyan, Y.; Beigang, R. *Opt. Lett.* **2001**, *26*, 563.
(133) Weiss, C.; Torosyan, G.; Meyn, J. P.; Wallenstein, R.; Beigang, R.; Avetisyan, Y. *Opt. Express* **2001**, *8*, 497.
(134) Hamster, H.; Sullivan, A.; Gordon, S.; White, W.; Falcone, R. W. *Phys. Rev. Lett.* **1993**, *71*, 2725.
(135) Hamster, H.; Sullivan, A.; Gordon, S.; Falcone, R. W. *Phys. Rev. E* **1994**, *49*, 671.
(136) Loffler, T.; Jacob, F.; Roskos, H. G. *Appl. Phys. Lett.* **2000**, *77*, 453.
(137) Cook, D. J.; Hochstrasser, R. M. *Opt. Lett.* **2000**, *25*, 1210.

(138) Chen, Q.; Jiang, Z. P.; Tani, M.; Zhang, X. C. *Electron. Lett.* **2000**, *36*, 1298.
(139) Chen, Q.; Tani, M.; Jiang, Z. P.; Zhang, X. C. *J. Opt. Soc. Am. B* **2001**, *18*, 823.
(140) Tani, M.; Jiang, Z. P.; Zhang, X. C. *Electron. Lett.* **2000**, *36*, 804.
(141) Greene, B. I.; Federici, J. F.; Dykaar, D. R.; Jones, R. R.; Bucksbaum, P. H. *Appl. Phys. Lett.* **1991**, *59*, 893.
(142) Prabhu, S. S.; Ralph, S. E.; Melloch, M. R.; Harmon, E. S. *Appl. Phys. Lett.* **1997**, *70*, 2419.
(143) Ralph, S. E.; Chen, Y.; Woodall, J.; McInturff, D. *Phys. Rev. B* **1996**, *54*, 5568.
(144) Nahata, A.; Heinz, T. F. *Opt. Lett.* **1998**, *23*, 67.
(145) Bromage, J.; Walmsley, I. A.; Stroud, C. R. *Appl. Phys. Lett.* **1999**, *75*, 2181.
(146) Jacobsen, R. H.; Birkelund, K.; Holst, T.; Jepsen, P. U.; Keiding, S. R. *J. Appl. Phys.* **1996**, *79*, 2649.
(147) Nemec, H.; Pashkin, A.; Kuzel, P.; Khazan, M.; Schnull, S.; Wilke, I. *J. Appl. Phys.* **2001**, *90*, 1303.
(148) Leitenstorfer, A.; Hunsche, S.; Shah, J.; Nuss, M. C.; Knox, W. H. *Phys. Rev. Lett.* **1999**, *82*, 5140.
(149) Leitenstorfer, A.; Hunsche, S.; Shah, J.; Nuss, M. C.; Knox, W. H. *Phys. Rev. B* **2000**, *61*, 16642.
(150) Markelz, A. G.; Heilweil, E. J. *Appl. Phys. Lett.* **1998**, *72*, 2229.
(151) Sekine, N.; Hirakawa, K.; Sogawa, F.; Arakawa, Y.; Usami, N.; Shiraki, Y.; Katoda, T. *Appl. Phys. Lett.* **1996**, *68*, 3419.
(152) Nakajima, M.; Takahashi, M.; Hangyo, M. *J. Lumin.* **2001**, *94*, 627.
(153) Nakajima, M.; Takahashi, M.; Hangyo, M. *Physica B* **2002**, *314*, 176.
(154) Xu, L.; Hu, B. B.; Xin, W.; Auston, D. H.; Morse, J. D. *Appl. Phys. Lett.* **1993**, *62*, 3507.
(155) Kersting, R.; Unterrainer, K.; Strasser, G.; Kauffmann, H. F.; Gornik, E. *Phys. Rev. Lett.* **1997**, *79*, 3038.
(156) Leitenstorfer, A.; Hunsche, S.; Shah, J.; Nuss, M. C.; Knox, W. H. *Physica B* **1999**, *272*, 348.
(157) Yu, P. Y.; Cardona, M. *Fundamentals of Semiconductors*; 3rd ed.; Springer: New York, 2001.
(158) Hirakawa, K.; Wilke, I.; Yamanaka, K.; Roskos, H. G.; Vosseburger, M.; Wolter, F.; Waschke, C.; Kurz, H.; Grayson, M.; Tsui, D. C. *Surf. Sci.* **1996**, *362*, 368.
(159) Sekine, N.; Hirakawa, K.; Vossebuerger, M.; Haring-Bolivar, P.; Kurz, H. *Microelectron. Eng.* **1999**, *47*, 289.
(160) Sekine, N.; Yamanaka, K.; Hirakawa, K.; Vosseburger, M.; Haring-Bolivar, P.; Kurz, H. *Appl. Phys. Lett.* **1999**, *74*, 1006.
(161) Sekine, N.; Hirakawa, K.; Vosseburger, M.; Haring-Bolivar, P.; Kurz, H. *Compd. Semicond. 1998, Proc. Int. Symp., 25th, 1998* **1999**, *162*.
(162) Planken, P. C. M.; Nuss, M. C.; Brener, I.; Goossen, K. W.; Luo, M. S. C.; Chuang, S. L.; Pfeiffer, L. *Phys. Rev. Lett.* **1992**, *69*, 3800.
(163) Planken, P. C. M.; Nuss, M. C.; Knox, W. H.; Miller, D. A. B.; Goossen, K. W. *Appl. Phys. Lett.* **1992**, *61*, 2009.
(164) Planken, P. C. M.; Brener, I.; Nuss, M. C.; Luo, M. S. C.; Chuang, S. L.; Pfeiffer, L. N. *Phys. Rev. B* **1994**, *49*, 4668.
(165) Brener, I.; Planken, P. C. M.; Nuss, M. C.; Luo, M. S. C.; Chuang, S. L.; Pfeiffer, L.; Leaird, D. E.; Weiner, A. M. *J. Opt. Soc. Am. B* **1994**, *11*, 2457.
(166) Sha, W. J.; Rhee, J. K.; Norris, T. B.; Schaff, W. J. *IEEE J. Quantum Electron.* **1992**, *28*, 2445.
(167) Roskos, H. G.; Nuss, M. C.; Shah, J.; Leo, K.; Miller, D. A. B.; Fox, A. M.; Schmittrink, S.; Kohler, K. *Phys. Rev. Lett.* **1992**, *68*, 2216.
(168) Planken, P. C. M.; Brener, I.; Nuss, M. C.; Luo, M. S. C.; Chuang, S. L. *Phys. Rev. B* **1993**, *48*, 4903.
(169) Nuss, M. C.; Planken, P. C. M.; Brener, I.; Roskos, H. G.; Luo, M. S. C.; Chuang, S. L. *Appl. Phys. B* **1994**, *58*, 249.
(170) Luo, M. S. C.; Chuang, S. L.; Planken, P. C. M.; Brener, I.; Roskos, H. G.; Nuss, M. C. *IEEE J. Quantum Electron.* **1994**, *30*, 1478.
(171) Sekine, N.; Hirakawa, K.; Arakawa, Y. *Jpn. J. Appl. Phys., Part 1* **1998**, *37*, 1643.
(172) Morohashi, I.; Komori, K.; Hidaka, T.; Sugaya, T.; Wang, X. L.; Ogura, M.; Nakagawa, T.; Son, C. S. *Jpn. J. Appl. Phys., Part 1* **2001**, *40*, 3012.
(173) Camacho, A. S.; Gutierrez, R. M.; Bohorquez, J. *Phys. Status Solidi B* **2002**, *232*, 56.
(174) Morohashi, I.; Komori, K.; Wang, X. L.; Hidaka, T.; Ogura, M.; Watanabe, M. *Jpn. J. Appl. Phys., Part 1* **2002**, *41*, 2710.
(175) Zhang, W. M.; Meier, T.; Chernyak, V.; Mukamel, S. *Phys. Rev. B* **1999**, *60*, 2599.
(176) Waschke, C.; Leisching, P.; Bolivar, P. H.; Schwedler, R.; Bruggemann, F.; Roskos, H. G.; Leo, K.; Kurz, H.; Kohler, K. *Solid-State Electron.* **1994**, *37*, 1321.
(177) Waschke, C.; Roskos, H. G.; Leo, K.; Kurz, H.; Kohler, K. *Semicond. Sci. Technol.* **1994**, *9*, 416.
(178) Dekorsy, T.; Leisching, P.; Waschke, C.; Kohler, K.; Leo, K.; Roskos, H. G.; Kurz, H. *Semicond. Sci. Technol.* **1994**, *9*, 1959.
(179) Roskos, H. G. In *Festkorperprobleme-Advances in Solid State Physics*, 1995; Vol. 34.
(180) Dekorsy, T.; Ott, R.; Leisching, P.; Bakker, H. J.; Waschke, C.; Roskos, H. G.; Kurz, H.; Kohler, K. *Solid-State Electron.* **1996**, *40*, 551.
(181) Shimada, Y.; Matsuno, T.; Hirakawa, K. *Jpn. J. Appl. Phys., Part 1* **2001**, *40*, 3009.
(182) Shimada, Y.; Hirakawa, K.; Lee, S. W. *Appl. Phys. Lett.* **2002**, *81*, 1642.
(183) Sudzius, M.; Lyssenko, V. G.; Loser, F.; Leo, K.; Dignam, M. M.; Kohler, K. *Phys. Rev. B* **1998**, *57*, R12693.
(184) Shimada, Y.; Hirakawa, K. *Compd. Semicond. 2001* **2002**.
(185) Hokomoto, Y.; Kadoya, Y.; Yamanishi, M. *Appl. Phys. Lett.* **1999**, *74*, 3839.
(186) Sakurada, T.; Kadoya, Y.; Yamanishi, M. *Jpn. J. Appl. Phys., Part 2* **2002**, *41*, L256.
(187) Walecki, W. J.; Some, D.; Kozlov, V. G.; Nurmikko, A. V. *Appl. Phys. Lett.* **1993**, *63*, 1809.
(188) Some, D.; Nurmikko, A. V. *Appl. Phys. Lett.* **1994**, *65*, 3377.
(189) Kersting, R.; Bratschitsch, R.; Strasser, G.; Unterrainer, K.; Heyman, J. N. *Opt. Lett.* **2000**, *25*, 272.
(190) Ascazubi, R.; Akin, O. C.; Zaman, T.; Kersting, R.; Strasser, G. *Appl. Phys. Lett.* **2002**, *81*, 4344.
(191) Tonouchi, M.; Tani, M.; Wang, Z.; Sakai, K.; Tomozawa, S.; Hangyo, M.; Murakami, Y.; Nakashima, S. I. *Jpn. J. Appl. Phys., Part 1* **1996**, *35*, 2624.
(192) Tonouchi, M.; Tani, M.; Wang, Z.; Sakai, K.; Wada, N.; Hangyo, M. *Jpn. J. Appl. Phys., Part 2* **1996**, *35*, L1578.
(193) Hangyo, M.; Tomozawa, S.; Murakami, Y.; Tonouchi, M.; Tani, M.; Wang, Z.; Sakai, K.; Nakashima, S. *Appl. Phys. Lett.* **1996**, *69*, 2122.
(194) Jaekel, C.; Roskos, H. G.; Kurz, H. *Phys. Rev. B* **1996**, *54*, R6889.
(195) Jaekel, C.; Roskos, H. G.; Kurz, H. *IEEE Trans. Appl. Supercond.* **1997**, *7*, 3722.
(196) Tani, M.; Tonouchi, M.; Wang, Z.; Sakai, K.; Hangyo, M.; Tomozawa, S.; Murakami, Y. *Jpn. J. Appl. Phys., Part 2* **1996**, *35*, L1184.
(197) Tonouchi, M.; Tani, M.; Wang, Z.; Sakai, K.; Wada, N.; Hangyo, M. *Jpn. J. Appl. Phys., Part 2* **1997**, *36*, L93.
(198) Tonouchi, M.; Wada, N.; Shikii, S.; Hangyo, M.; Tani, M.; Sakai, K. *Physica C* **1997**, *293*, 82.
(199) Hangyo, M.; Wada, N.; Tonouchi, M.; Tani, M.; Sakai, K. *IEICE Trans. Electron.* **1997**, *E80C*, 1282.
(200) Hangyo, M.; Tomozawa, S.; Murakami, Y.; Tonouchi, M.; Tani, M.; Wang, Z.; Sakai, K. *IEEE Trans. Appl. Supercond.* **1997**, *7*, 2909.
(201) Hangyo, M.; Tomozawa, S.; Murakami, Y.; Tonouchi, M.; Tani, M.; Wang, Z.; Sakai, K. *IEEE Trans. Appl. Supercond.* **1997**, *7*, 3730.
(202) Iguchi, I.; Kume, E.; Takahashi, H. *Phys. Rev. B* **2000**, *62*, 5370.
(203) Wald, H.; Steigmeier, C.; Seidel, P.; Nashima, S.; Tonouchi, M.; Hangyo, M. *Physica C* **2000**, *341*, 1899.
(204) Yoshimura, T.; Kiwa, T.; Tonouchi, M. *Physica C* **2001**, *362*, 329.
(205) Wald, H.; Seidel, P.; Tonouchi, M. *Physica C* **2002**, *367*, 308.
(206) Wald, H.; Seidel, P.; Tonouchi, M. *Physica C* **2001**, *362*, 324.
(207) Wald, H.; Seidel, P.; Tonouchi, M. *Physica C* **2001**, *357*, 146.
(208) Wald, H.; Schmidt, F.; Seidel, P.; Tonouchi, M. *Supercond. Sci. Technol.* **2002**, *15*, 1494.
(209) Tominari, Y.; Kiwa, T.; Murakami, H.; Tonouchi, M.; Wald, H.; Seidel, P.; Schneidewind, H. *Appl. Phys. Lett.* **2002**, *80*, 3147.
(210) Tominari, Y.; Kiwa, T.; Murakami, H.; Tonouchi, M.; Wald, H.; Seidel, P.; Schneidewind, H. *Physica C* **2003**, *388*, 481.
(211) Beard, M. C.; Turner, G. M.; Schmuttenmaer, C. A. *J. Am. Chem. Soc.* **2000**, *122*, 11541.
(212) Beard, M. C.; Turner, G. M.; Schmuttenmaer, C. A. *J. Phys. Chem. A* **2002**, *106*, 878.
(213) Groot, M. L.; Vos, M. H.; Schlichting, I.; van Mourik, F.; Joffre, M.; Lambry, J. C.; Martin, J. L. *Proc. Natl. Acad. Sci. U.S.A.* **2002**, *99*, 1323.
(214) Kida, N.; Tonouchi, M. *Appl. Phys. Lett.* **2001**, *78*, 4115.
(215) Kida, N.; Tonouchi, M. *Appl. Phys. Lett.* **2003**, *82*, 3412.
(216) Wilke, I.; MacLeod, A. M.; Gillespie, W. A.; Berden, G.; Knippels, G. M. H.; van der Meer, A. F. G. *Nucl. Instrum. Methods Phys. Res., Sect. A* **2002**, *483*, 282.
(217) Wilke, I.; MacLeod, A. M.; Gillespie, W. A.; Berden, G.; Knippels, G. M. H.; van der Meer, A. F. G. *Phys. Rev. Lett.* **2002**, *88*, 124801.
(218) Pedersen, J. E.; Lyssenko, V. G.; Hvam, J. M.; Jepsen, P. U.; Keiding, S. R.; Sorensen, C. B.; Lindelof, P. E. *Appl. Phys. Lett.* **1993**, *62*, 1265.
(219) Brorson, S. D.; Zhang, J. C.; Keiding, S. R. *Appl. Phys. Lett.* **1994**, *64*, 2385.
(220) Hu, B. B.; Desouza, E. A.; Knox, W. H.; Cunningham, J. E.; Nuss, M. C.; Kuznetsov, A. V.; Chuang, S. L. *Phys. Rev. Lett.* **1995**, *74*, 1689.
(221) Taylor, A. J.; Rodriguez, G.; Some, D. *Opt. Lett.* **1997**, *22*, 715.
(222) Huggard, P. G.; Cluff, J. A.; Shaw, C. J.; Andrews, S. R.; Linfield, E. H.; Ritchie, D. A. *Appl. Phys. Lett.* **1997**, *71*, 2647.
(223) Kersting, R.; Heyman, J. N.; Strasser, G.; Unterrainer, K. *Phys. Rev. B* **1998**, *58*, 4553.

(224) Tonouchi, M.; Kawasaki, N.; Yoshimura, T.; Wald, H.; Seidel, P. *Jpn. J. Appl. Phys., Part 2* **2002**, *41*, L706.
(225) Weling, A. S.; Hu, B. B.; Froberg, N. M.; Auston, D. H. *Appl. Phys. Lett.* **1994**, *64*, 137.
(226) Weling, A. S.; Auston, D. H. *J. Opt. Soc. Am. B* **1996**, *13*, 2783.
(227) Liu, Y. Q.; Park, S. G.; Weiner, A. M. *Opt. Lett.* **1996**, *21*, 1762.
(228) Siders, C. W.; Siders, J. L. W.; Taylor, A. J.; Park, S. G.; Melloch, M. R.; Weiner, A. M. *Opt. Lett.* **1999**, *24*, 241.
(229) Sohn, J. Y.; Ahn, Y. H.; Park, D. J.; Oh, E.; Kim, D. S. *Appl. Phys. Lett.* **2002**, *81*, 13.
(230) Haran, G.; Sun, W. D.; Wynne, K.; Hochstrasser, R. M. *Chem. Phys. Lett.* **1997**, *274*, 365.
(231) McElroy, R.; Wynne, K. *Phys. Rev. Lett.* **1997**, *79*, 3078.
(232) Greene, B. I.; Federici, J. F.; Dykaar, D. R.; Levi, A. F. J.; Pfeiffer, L. *Opt. Lett.* **1991**, *16*, 48.
(233) Saeta, P. N.; Federici, J. F.; Greene, B. I.; Dykaar, D. R. *Appl. Phys. Lett.* **1992**, *60*, 1477.
(234) Chen, Y.; Prabhu, S. S.; Ralph, S. E.; McInturff, D. T. *Appl. Phys. Lett.* **1998**, *72*, 439.
(235) Messner, C.; Kostner, H.; Hopfel, R. A.; Unterrainer, K. *J. Opt. Soc. Am. B* **2001**, *18*, 1369.
(236) Lui, K. P. H.; Hegmann, F. A. *Appl. Phys. Lett.* **2001**, *78*, 3478.
(237) Lui, K. P. H.; Hegmann, F. A. *J. Appl. Phys.* **2003**, *93*, 9012.
(238) Jepsen, P. U.; Schairer, W.; Libon, I. H.; Lemmer, U.; Hecker, N. E.; Birkholz, M.; Lips, K.; Schall, M. *Appl. Phys. Lett.* **2001**, *79*, 1291.
(239) Yarotski, D. A.; Averitt, R. D.; Negre, N.; Crooker, S. A.; Taylor, A. J.; Donati, G. P.; Stintz, A.; Lester, L. F.; Malloy, K. J. *J. Opt. Soc. Am. B* **2002**, *19*, 1480.
(240) Segschneider, G.; Jacob, F.; Loffler, T.; Roskos, H. G.; Tautz, S.; Kiesel, P.; Dohler, G. *Phys. Rev. B* **2002**, *65*, 125205.
(241) Hegmann, F. A.; Tykwinski, R. R.; Lui, K. P. H.; Bullock, J. E.; Anthony, J. E. *Phys. Rev. Lett.* **2002**, *89*, 227403.
(242) Stanton, C. J.; Bailey, D. W. *Phys. Rev. B* **1992**, *45*, 8369.
(243) Federici, J. F.; Greene, B. I.; Saeta, P. N.; Dykaar, D. R.; Sharifi, F.; Dynes, R. C. *Phys. Rev. B* **1992**, *46*, 11153.
(244) Groeneveld, R. H. M.; Grischkowsky, D. *J. Opt. Soc. Am. B* **1994**, *11*, 2502.
(245) Flanders, B. N.; Arnett, D. C.; Scherer, N. F. *IEEE J. Sel. Top. Quantum Electron.* **1998**, *4*, 353.
(246) Schall, M.; Jepsen, P. U. *Opt. Lett.* **2000**, *25*, 13.
(247) Knoesel, E.; Bonn, M.; Shan, J.; Heinz, T. F. *Phys. Rev. Lett.* **2001**, *86*, 340.
(248) Jamison, S. P.; Shen, J. L.; Jones, D. R.; Issac, R. C.; Ersfeld, B.; Clark, D.; Jaroszynski, D. A. *J. Appl. Phys.* **2003**, *93*, 4334.
(249) Nuss, M. C.; Auston, D. H.; Capasso, F. *Phys. Rev. Lett.* **1987**, *58*, 2355.
(250) Zielbauer, J.; Wegener, M. *Appl. Phys. Lett.* **1996**, *68*, 1223.
(251) Huber, R.; Tauser, F.; Brodschelm, A.; Bichler, M.; Abstreiter, G.; Leitenstorfer, A. *Nature* **2001**, *414*, 286.
(252) Huber, R.; Tauser, F.; Brodschelm, A.; Bichler, M.; Abstreiter, G.; Leitenstorfer, A. *J. Lumin.* **2001**, *94*, 555.
(253) Huber, R.; Tauser, F.; Brodschelm, A.; Leitenstorfer, A. *Phys. Status Solidi B* **2002**, *234*, 207.
(254) Leitenstorfer, A.; Huber, R.; Tauser, F.; Brodschelm, A.; Bichler, M.; Abstreiter, G. *Physica B* **2002**, *314*, 248.
(255) Kaindl, R. A.; Carnahan, M. A.; Hagele, D.; Lovenich, R.; Chemla, D. S. *Nature* **2003**, *423*, 734.
(256) Averitt, R. D.; Rodriguez, G.; Siders, J. L. W.; Trugman, S. A.; Taylor, A. J. *J. Opt. Soc. Am. B* **2000**, *17*, 327.
(257) Averitt, R. D.; Rodriguez, G.; Lobad, A. I.; Siders, J. L. W.; Trugman, S. A.; Taylor, A. J. *Phys. Rev. B* **2001**, *63*, 140502.
(258) Brorson, S. D.; Buhleier, R.; Trofimov, I. E.; White, J. O.; Ludwig, C.; Balakirev, F. F.; Habermeier, H. U.; Kuhl, J. *J. Opt. Soc. Am. B* **1996**, *13*, 1979.
(259) Averitt, R. D.; Lobad, A. I.; Kwon, C.; Trugman, S. A.; Thorsmolle, V. K.; Taylor, A. J. *Phys. Rev. Lett.* **2001**, *87*, 017401.
(260) Beard, M. C.; Schmuttenmaer, C. A. *J. Chem. Phys.* **2001**, *114*, 2903.
(261) Beard, M. C.; Turner, G. M.; Schmuttenmaer, C. A. *Liquid Dynamics: Experiment, Simulation, and Theory*, 2002; Vol. 820.
(262) Beard, M. C.; Turner, G. M.; Schmuttenmaer, C. A. *Nano Lett.* **2002**, *2*, 983.
(263) Turner, G. M.; Beard, M. C.; Schmuttenmaer, C. A. *J. Phys. Chem. B* **2002**, *106*, 11716.
(264) Smith, N. V. *Phys. Rev. B* **2001**, *64*, 155106.
(265) Cook, D. J.; Chen, J. X.; Morlino, E. A.; Hochstrasser, R. M. *Chem. Phys. Lett.* **1999**, *309*, 221.
(266) Ahn, J.; Hutchinson, D. N.; Rangan, C.; Bucksbaum, P. H. *Phys. Rev. Lett.* **2001**, *86*, 1179.
(267) Ahn, J.; Rangan, C.; Hutchinson, D. N.; Bucksbaum, P. H. *Phys. Rev. A* **2002**, *66*, 022312.
(268) Jones, R. R.; You, D.; Bucksbaum, P. H. *Phys. Rev. Lett.* **1993**, *70*, 1236.
(269) Jones, R. R.; Tielking, N. E.; You, D.; Raman, C.; Bucksbaum, P. H. *Phys. Rev. A* **1995**, *51*, R2687.
(270) Raman, C.; Conover, C. W. S.; Sukenik, C. I.; Bucksbaum, P. H. *Phys. Rev. Lett.* **1996**, *76*, 2436.
(271) Raman, C.; Weinacht, T. C.; Bucksbaum, P. H. *Phys. Rev. A* **1997**, *55*, R3995.
(272) Rangan, C.; Bucksbaum, P. H. *Phys. Rev. A* **2001**, *64*, 033417.
(273) Rangan, C.; Ahn, J.; Hutchinson, D. N.; Bucksbaum, P. H. *J. Mod. Opt.* **2002**, *49*, 2339.
(274) Reinhold: C. O.; Burgdorfer, J.; Jones, R. R.; Raman, C.; Bucksbaum, P. H. *J. Phys. B* **1995**, *28*, L457.
(275) Manescu, C.; Krause, J. L.; Schafer, K. J. *Phys. Rev. A* **2003**, *68*.
(276) Hache, A.; Kostoulas, Y.; Atanasov, R.; Hughes, J. L. P.; Sipe, J. E.; vanDriel, H. M. *Appl. Phys. Lett.* **1997**, *78*, 306.
(277) Kral, P.; Sipe, J. E. *Phys. Rev. B* **2000**, *61*, 5381.
(278) Cote, D.; Fraser, J. M.; DeCamp, M.; Bucksbaum, P. H.; van Driel, H. M. *Appl. Phys. Lett.* **1999**, *75*, 3959.
(279) Cote, D.; Laman, N.; van Driel, H. M. *Appl. Phys. Lett.* **2002**, *80*, 905.
(280) Jepsen, P. U.; Keiding, S. R. *Opt. Lett.* **1995**, *20*, 807.
(281) Joshi, R. P.; Dharamsi, A. N. *J. Appl. Phys.* **1993**, *74*, 3215.
(282) Khurgin, J. B. *J. Opt. Soc. Am. B* **1994**, *11*, 2492.
(283) Abe, M.; Madhavi, S.; Shimada, Y.; Otsuka, Y.; Hirakawa, K.; Tomizawa, K. *Appl. Phys. Lett.* **2002**, *81*, 679.
(284) Piao, Z. S.; Tani, M.; Sakai, K. *Jpn. J. Appl. Phys., Part 1* **2000**, *39*, 96.
(285) You, D.; Bucksbaum, P. H. *J. Opt. Soc. Am. B* **1997**, *14*, 1651.
(286) Kuzel, P.; Khazan, M. A.; Kroupa, J. *J. Opt. Soc. Am. B* **1999**, *16*, 1795.
(287) Nekkanti, S.; Sullivan, D.; Citrin, D. S. *IEEE J. Quantum Electron.* **2001**, *37*, 1226.
(288) Nemec, H.; Kadlec, F.; Kuzel, P. *J. Chem. Phys.* **2002**, *117*, 8454.
(289) Cote, D.; Sipe, J. E.; van Driel, H. M. *J. Opt. Soc. Am. B* **2003**, *20*, 1374.
(290) Lachaine, J. M.; Hawton, M.; Sipe, J. E.; Dignam, M. M. *Phys. Rev. B* **2000**, *62*, R4829.
(291) Okumura, K.; Tanimura, Y. *Chem. Phys. Lett.* **1998**, *295*, 298.
(292) Kindt, J. T.; Schmuttenmaer, C. A. *J. Chem. Phys.* **1999**, *110*, 8589.
(293) Feise, M. W.; Citrin, D. S. *Appl. Phys. Lett.* **1999**, *75*, 3536.
(294) Asplund, M. C.; Zanni, M. T.; Hochstrasser, R. M. *Proc. Natl. Acad. Sci. U.S.A.* **2000**, *97*, 8219.
(295) Golonzka, O.; Khalil, M.; Demirdoven, N.; Tokmakoff, A. *Phys. Rev. Lett.* **2001**, *86*, 2154.
(296) Hybl, J. D.; Albrecht, A. W.; Faeder, S. M. G.; Jonas, D. M. *Chem. Phys. Lett.* **1998**, *297*, 307.
(297) Cook, D. J. Personal communication, 2003.
(298) Dlott, D. D. *Annu. Rev. Phys. Chem.* **1986**, *37*, 157.
(299) Beard, M. C.; Turner, G. M.; Murphy, J. E.; Micic, O. I.; Hanna, M. C.; Nozik, A. J.; Schmuttenmaer, C. A. *Nano Lett.* **2003**, *3*, 1695.
(300) Service, R. F. *Science* **2003**, *302*, 556.
(301) Beaurepaire, E.; Turner, G. M.; Harrel, S. M.; Beard, M. C.; Bigot, J.-Y.; Schmuttenmaer, C. A. *Appl. Phys. Lett.*, submitted for publication.

CR020685G